CHALMERS

Pairing Based Implementation of a Fat-Saturation in a Balanced SSFP MR-Sequence

Master of Science Thesis in Electrical Engineering

CHRISTOPH ULLISCH

Department of Signals and Systems
Division of Biomedical Engineering
CHALMERS UNIVERSITY OF TECHNOLOGY
Göteborg, Sweden, 2010
Report No. EX082/2010

Master Thesis EX082/2010

Pairing Based Implementation of a Fat-Saturation in a Balanced SSFP MR-Sequence

CHRISTOPH ULLISCH

Pairing Based Implementation of a Fat-Saturation Implementation
in a Balanced SSFP MR-Sequence

CHRISTOPH O. ULLISCH

Master Thesis EX082/2010

Department of Signals and Systems
Division of Biomedical Engineering
CHALMERS UNIVERSITY OF TECHNOLOGY
SE-41296 Göteborg
Sweden
Telephone +46 (0) 31-772 1000

Abstract

Pairing Based Implementation of a Fat-Saturation
in a Balanced SSFP MR-Sequence

Pairing is a method developed by O. Bieri (1) to reduced eddy current artefacts in balanced SSFP MR-sequences. In this thesis a frequency selective fat-saturation based on the pairing principle was implemented. The intention was to achieve a more flexible configuration, with arbitrary localization of the fat-saturation in the k-space during the acquisition and probably potential to reduce SAR. For this purpose the IDEA-FLASH sequence, provided from Siemens Erlangen, Germany, for MR-sequence development, was modified to a balanced SSFP sequence. The result was compared to the TrueFisp product sequence, without major differences. In the modified sequence hence a pair of identical fat-saturation TR´s where implemented, with the possibility of several parameter variations. For optimization, series with parameter variations were performed. As an optimum was achieved, it was compared with the product solution. The pairing did reduce the eddy current artefacts, but there where still some eddy current artefacts left. In addition there was a lack in spoiling of the fat-signal, which reduced the image quality below requirements of diagnostic imaging. Never the less an additional synergetic effect of paired fat saturation pulses occurred, which could be worth to investigate by simulations, due to the potential of reducing SAR.

Key word: Pairing, TrueFisp, balanced SSFP, fat-saturation, eddy currents, MR-sequence development

Christoph O. Ullisch

Department of Signals and Systems
CHALMERS UNIVERSITY OF TECHNOLOGY

and

Division of Radiological Physics
UNIVERSITY HOSPITAL AND UNIVERSITY BASEL

Table of Contents

Preface

This master thesis was written to achieve the master in electrical and biomedical engineering at the Chalmers University of Technology, Göteborg, Sweden. The intention of the author was to become familiar with the sequence development techniques on clinical MR-scanners. The practical work with sequence programming and sequence testing were carried out at the Division of Radiological Physics at the University Hospital and University Basel, in Basel Switzerland during autumn 2008 to summer 2009. The theoretical preparations before the work in Basel and the writing afterwards were located in Göteborg, Sweden.

Special thanks are directed to Professor Klaus Scheffler, the head of the Radiological Physics in Basel, first of all because he was one of few, who thought it could be possible to offer a MR-sequence programming topic in the scope of a master thesis and further more for the supervision and the time at the scanner during the thesis. Oliver Bieri for providing me with relevant papers and answers taken from his astonishing physic all-round knowledge. Sunil Patil for the introduction to sequence programming and help during the programming task. Markus Klarhöfer for help in the most frenetic debugging phase to transfer my sequence to VA13. Henk-Joost Crooijmans for the support at the most frenetic measuring day with his slot at the scanner and providing me with a healthy knee. Permi Jhooti for the linguistic support. Francesco Santini for the help and encouraging to ask by the sentence "You medical guys always want to read it by you self instead of asking others – which is quicker", what I did afterwards. Claudia Lenz, Monika Gloor, Jan-Ole Blumenhagen, as well as the other members of the group for the helpful and good atmosphere during my work in Basel. Seline Schellenberg who managed the major part of the administrative processes in Switzerland. My brother Marcus Ullisch at the MR Physics in Jülich for providing me with literature and software tips. Professor Mikael Persson, head of the Division Biomedical Engineering, Chalmers University of Technology, Göteborg, Sweden, for supporting the thesis as examinator.

Göteborg December 2010

Christoph Ullisch

Notations

$\mathbf{B}_0$	Static longitudinal magnetic field in the scanner
$\mathbf{B}_1$	Rotating transversal magnetic field in the scanner
f	Frequency
G	Gradient
k	Wave number
M	Net magnetization of the spins
M_{xy}	Transverse magnetization component of **M**
M_z	Longitudinal magnetization component of **M**
r	Distance vector
S	Spin angular moment
T_1	Spin lattice time constant
T_2	Spin spin time constant
TE	Echo time
TR	Repetition time
α	Flip angle
γ	Gyro magnetic ratio
ϕ	Phase
μ	Magnetic moment
ω	Angular frequency
Δt	Duration
Δs	Bandwidth

Abreviations

FID	Free-induction decay
FLASH	Fast low-angle shot
MR	Magnetic resonance
RF	Radio frequency
SSFP	Steady State Free Precision

1 Introduction

The subject of this master thesis is the implementation of an intermitted fat saturation in a Steady State Free Precision Sequence (SSFP-Sequence). Intermitted is, in this case, the fact that the fat saturation pulse is played out arbitrary during the acquisition mean whilst the spins are excited. The benefit of an intermitted fat saturation would be a more flexible scheme of fat saturation pulses, which could lead to a reduction of both time and specific absorption rate (SAR). An approach of the reduction of the steady state disturbance and eddy current artefacts is the implementation of the pairing principle developed by O. Bieri et al.(1), where the fat saturation pulse is played out twice in a row to reduce the eddy current artefacts. The development has been done on Siemens scanners with the IDEA-sequence-development-tool. Starting from the IDEA-Flash-sequence, which is delivered with the IDEA package, the first steps were to program a balanced SSFP-sequence. A major part of this programming modification was the balancing of all gradients in the time of repetition interval (TR-interval). The benefits i.e. time reduction and decreased SAR would be highest in 3D imaging due to the higher numbers of repeated excitation in a shorter time interval. This required the implementation of the 3D-acquisition on the derived balanced SSFP-sequence. The next step was to implement an own fat saturation function with a large number of variables, which had to be adjustable in the user interface on the scanner for quick and flexible measurement setup. The measurements where performed on phantoms containing three bottles - the Siemens water phantom and the two others filled with food oil. Finally, a measurement of a knee from a healthy volunteer was performed to verify the result.

2 Theory

2.1 Basic MR-theory

Even the study of several reputable MR-literatures (2-7) gives the impression of a slight incoherence in the explanation of the MR-theory. Hanson (2) gives a good explanation for that fact and claims it is caused by mixing both quantum mechanics and classic mechanics motivated by the attempt to simplify the complex mater, which finally in some cases results in wrong statements. He also states that classic mechanics is in most cases sufficient to explain the physics for a MR-image acquisition, so is even the case for this thesis. This chapter explains by quantum mechanics how the magnetization-vector is achieved in a MR-scanner, while the explanation of the manipulation of the magnetization sticks strictly to the classic explanation. (2)

The main precondition for achieving an MR-signal from a nucleus is an odd number of protons and/or odd number of neutrons hence only those nuclei possess a net spin angular moment. ^{1}H, ^{13}C, ^{19}F, ^{23}Na and ^{31}P are examples for those nuclei. As described later the magnetization vector of these nuclei placed in a magnetic field rotates and the rotation has different frequencies for the different nuclei. As ^{1}H by far is the most

frequent atom in a human body, the standard medical MR-imaging is based on the hydrogen-atom. (2, 3)

As mentioned above the spin angular moment – often only called spin - of a nucleus is the base for MR-imaging. A classic angular moment is a quantity of a rotating object and is a vector in the direction of the rotation axis with positive/negative orientation according to the right hand rule. I.e. the thumb is pointing at the positive direction if the other fingers of the right hand are pointing at the perpendicular rotation direction. In quantum mechanics a spin angular moment of a particle is not caused by a rotation. It is an intrinsic property of the particle like mass, electric charge or magnetism. The only difference is, that spin has no macroscopic correlate like the other intrinsic properties and is hence more difficult to grasp. The spin is a vector quantity and has the symbol **S**. The spin angular moment or the spin is a linear combination of the two spin eigenstates, which are called spin-up and spin-down. Only if a single nuclear spin is examined, like in a Stern-Gerlach-Experiment (8) the nucleus has either a single spin-down or spin-up. When an object with several protons in a smaller volume is examined the spin orientations are arbitrary, spherical, randomly distributed. The spin of a single proton in the volume is a superposition of the eigenstates spin-up and spin-down. This can result in an arbitrary direction of the spin. Despite their names the eigenstates spin-up and spin-down have even a transverse component and not only a longitudinal component. Every proton has an intrinsic nuclear magnetic moment **μ**. It is associated to the spin by the gyro magnetic ratio γ.

$$\mu = \gamma \cdot S$$

Equation 2.1

The gyro magnetic ratio is a property of the atomic nuclei and is 42.575 MHz/T for ^{1}H-atoms.

The integral of the intrinsic magnetic moment gives a net magnetization generated from all protons in the whole volume:

$$M = \sum \mu$$

Equation 2.2

In the absence of an external magnetic field, there is no net magnetization due to the spherical random distribution of the spins.

This can be changed by interactions of the nuclei with external magnetic fields. To be more exact by both types of magnetic fields, i.e. static magnetic field and radiofrequency (RF) fields. (2, 3)

If a large magnetic field $\mathbf{B}_0$ is applied over the volume of protons, the distribution of the spins **S** and hence the intrinsic magnetic moment, is no longer randomly spherical. There is a tendency of the spins to divert in the same direction as the static magnetic field $\mathbf{B}_0$ – to emphasize it once again it is only a slight change of the distribution and not a strict parallel and anti-parallel lining up of the spins. This generates a small net magnetization **M** in the same direction as the static magnetic field. By convention the direction of the static magnetic field is called the longitudinal or z-direction and the component of the magnetization **M** in this direction is called the longitudinal direction

M_z. According to that the perpendicular magnetization component is called the transversal magnetization M_{xy}. In clinical MR-scanners the static magnetic field is produced by supra-conduction coil, which is cooled by helium to nearly 0°K. The most common strengths of the field in clinically used scanners are 1.5 and 3T.

If the magnetization vector **M** is forced out of the longitudinal direction the static magnetic field $\mathbf{B}_0$ will, after classical mechanics, apply a torque on **M**. This torque can be calculated by **M** x $\mathbf{B}_0$. From the fact that force equals the rate of linear moment it can be reveald, that the equation of torque must equal the rate of change of angular moment over time.

$$\sum \frac{dS}{dt} = M \times B_0$$

Equation 2.3

From the Equation 2.1 we get the following equation by multiplying both sides by γ:

$$\frac{dM}{dt} = M \times \gamma B_0$$

Equation 2.4

The solution for this differential equation is a precession (rotation) of **M** around $\mathbf{B}_0$ as long as **M** has a transversal component, at a frequency given by:

$$\omega = \gamma B_0$$

Equation 2.5

This frequency ω is called the Lamor frequency and an important parameter in magnetic resonance processes. Actually, this frequency is the resonance frequency that other radiofrequency field must have to interact with the magnetization vector **M**. The radiofrequency field in the scanner is produced by an RF-coil, which produces a magnetic field $\mathbf{B}_1$. $\mathbf{B}_1$ is perpendicular to $\mathbf{B}_0$ and rotates at the Lamor frequency around the axis of $\mathbf{B}_0$. The $\mathbf{B}_1$ field rotates the magnetization away from the z-axis, giving **M** a transversal component M_{xy}. The angle between $\mathbf{B}_0$ and **M**, is called the flip-angle of the RF-pulse. After shutting down the current on the RF-coil, the magnetization vector **M** will continue precession around $\mathbf{B}_0$. The transversal component M_{xy} generates a current in the RF-coil, which can be registered as a signal. This is actually the signal used to process the image on a medical MR-scanner. After the excitation of the spins and hence flipping **M**, the transversal component M_{xy} will decline during precession, resulting in a decaying of the collected signal in the RF-coil. Even the longitudinal component M_z will re-grow until the vector **M** finally has only a longitudinal component in the thermal equilibrium, lining up parallel to $\mathbf{B}_0$. This phenomenon is called relaxation. (4, 5)

The longitudinal magnetization relaxation has the following differential equation:

$$\frac{dM_z}{dt} = \frac{M_z - M_0}{T_1}$$

Equation 2.6

, which has the solution:

$$M_z = M_0 + (M_z(0) - M_0)e^{-t/T_1}$$

Equation 2.7

T_1 is the spin-lattice time constant. It is a parameter related to the energy exchange between nuclei and the surrounding lattice.

The transversal magnetization relaxation has following differential equation:

$$\frac{dM_{xy}}{dt} = -\frac{M_{xy}}{T_2}$$

Equation 2.8

, which has the solution:

$$M_{xy} = M_{xy}(0) \cdot e^{-t/T_2}$$

Equation 2.9

T_2 is the spin-spin time constant. (4, 5)

Combination of Equation 2.4, Equation 2.6and Equation 2.8 gives the Bloch-equation Equation 2.10, which describes the time evolution of a magnetization placed in an external magnetic field. The diffusion component of the Bloch equation has been neglected, due to minor relevance in the project of this thesis: (5)

$$\frac{dM}{dt} = M \times \gamma B - \frac{M_x + M_y}{T_2} + \frac{M_0 - M_z}{T_1}$$

Equation 2.10: Bloch equation

2.2 Fat Saturation Techniques and Chemical Shift

The contrast in standard MR-imaging is dependant on the differences of T_1 and T_2 relaxation time in different tissues. An extension of the contrast variation can be reached by magnetization preparation. Magnetization preparation means a manipulation of the tissue magnetization before the excitation for signal resonance-generation.

Some of those magnetization preparations are aimed to eliminate the high signal of fat in medical MR-images, which is wanted to see other bright signal giving structures like oedema or contrast enhancement in fat containing tissue. There are several techniques for reducing the fat-signal, most of which use the chemical shift of the protons in the fat.

Chemical shift is a variation of the resonant frequency of protons caused by the bindings to different chemical structures. The electrons in the orbital around the nucleus cause a shielding of the nucleus to the static magnetic field $\mathbf{B}_0$, i.e. the field affecting the nucleus differs slightly from the static field and causes after the relation $\omega = \gamma\mathbf{B}_0$ a different Lamor frequency. The frequency difference is called the offset frequency $\omega_{off\text{-}set}$. The CH_2

groups in fat or lipids have an attraction of the electrons to the carbon. In free water the oxygen causes a higher attraction to the electrons then the carbon in the CH_2 groups. The electron shielding of the proton in the CH_2 group is more efficient causing a lower resonant frequency in the fat related protons. Fat also contains other carbohydrate groups and in average the resonant frequency is about 3.5 ppm lower compared to water. This phenomenon is used for a magnetization preparation called spectral-selective pre-pulse. I.e. before starting the pulse and gradient variation to acquire the signal for the image a pulse is given to force the magnetization vector of the fat tissue in the transversal plane. For this purpose the pre-pulse must be selective with a frequency of 3.5 ppm lower than the water frequency. This is according to the gyro magnetic ratio for water of 42.575 MHz/T an offset of 223,5 Hz at 1.5 T or 447 Hz at 3 T. The pre-pulse is followed by an additional small, spatial linearly varying, static magnetic field over a shorter time, which is called a gradient. The gradient causes a variation of the resonant frequency, which after deactivation leaves the protons with spins in different phase but same frequency, resulting in a smaller magnetization vector of the fat signal – the procedure is called spoiling and described in a own chapter below. After the pre-pulse is given and the magnetization vector of the fat tissue is in the transversal plane, a normal, more unselective excitation pulse, which covers both the fat and the water frequency, is given. This will flip the fat tissue magnetization vector from the transversal plan into the longitudinal plane in the opposite direction to the static field $\mathbf{B}_0$. The magnetization vector of the fat tissue will no longer contribute to the recorded signal by the lack of transversal magnetization. This phenomenon is also called saturation and hence the pre-pulse is called saturation pulse. The saturation normally last for 200 ms until the fat tissue magnetization vector gets back into thermal equilibrium, pointing parallel to $\mathbf{B}_0$. (4, 6)

Theoretically it would be preferable to give a fat-saturation pulse with short duration and narrow frequency spectrum. But in practice this can't be realized. It is not possible to choose both the pulse duration and the frequency spectrum arbitrary due to the uncertainty relation. This uncertainly relation is stated in the bandwidth-duration product. This mathematical phenomenon is based on the time and frequency interdependency and the product of the duration Δt and the frequency spectrum is $\Delta\omega$ or Δf is higher than a certain value. For a Gauss-pulse as used in the fat-saturation in this thesis the bandwidth-duration product has the following relation:

$$\Delta t \cdot \Delta f \approx 2.8$$

Equation 2.11

This relation gives following table of frequency offset for the different fat saturation pulse durations of the fat-saturation pulse:

Δt / *ms*	Δf / *Hz*
1	2800
2	1400
3	933
4	700
5	560
6	466
7	400

Table 2.1: Listed corresponding bandwidth for pulse durations from 1 to 7 *ms*

(5, 9)

2.3 Spatial Encoding and 3D-Imaging

The initial theory chapter explained how a MR-signal is achieved from a tissue containing protons. But, in MR-imaging, not even the signal generation is of great importance. For imaging the signal components must be traced to the different spatial locations. For this purpose a gradient of the magnetic field is produced after the RF-excitation for phase and frequency coding, to give the emitted RF-signal from different spins from different location a variation in the frequency and phase. By analysis of the RF-signal frequency components and phases of those components a tracing of the components to a spatial location is possible with the mathematical tool Fourier Transform.

A gradient is a small spatial fading magnetic field, which is added to the large static magnetic field $\mathbf{B}_0$. The gradient is produced by an additional coil-assembly system in the scanner and can establish a gradient in arbitrary directions inside the main helium cooled coil. The gradient is mathematical given by the equation:

$$G = \frac{dB}{dr}$$

Equation 2.12

And hence has the dimension *T/m*. For recent medical scanners the maximal gradient amplitude is about 25 – 60 *mT/m*. Another important technical specification is the rise time, i.e. the time it takes for the gradient coil system to establish the gradient amplitude after switching it on. By changing the amplitude of the magnetic field at different locations the gradient will result in different resonance frequencies at different locations.

Depending at which time during the image acquisition the gradients are switched on, the gradients have different functions and names. Slice selection gradients are placed at the same time as the RF-excitation pulse. By that only a slice with the matching resonance frequency is excited and not the whole sample inside the main coil. Phase encoding gradients are located between the RF-excitation and the readout. By that the spins

located at the higher field location proceed longer in the phase, while they have the same frequency at the start of the read out, when the gradient is deactivated again. Frequency encoding gradients are activated during the readout of the emitted resonance signal and cause a different frequency of the spins at different locations with higher frequencies at locations with higher magnetic field strength. Most common is a setup where phase and frequency encoding directions are perpendicular to each other. In the case of 3D imaging even a second phase encoding direction is added, which is perpendicular to the other two encoding directions. The recorded signal s(t) has in this case contributions from all the locations in the examined 3D-volume. The contribution is described by the 3D Fourier transformation:

$$s(t) = \int_x \int_y \int_z m(x,y,z) \cdot e^{-2\pi k_x(t)x} e^{-2\pi k_y(t)y} e^{-2\pi k_z(t)z} dxdydz$$

Equation 2.13

Where k(t) is given by:

$$k_x(t) = \frac{\gamma}{2\pi} \int_0^t G_x(\tau) d\tau$$

Equation 2.14

Inverse Fourier transformation can split the signal up to a signal for each voxel (small volume element). k is the wave number and seen from the formula above the gradients are determining the k-values. The assembly of the different k-values from the different gradient steps is also called the k-space. The advantage of the 3D acquisition is that every point in the k-space is contributing to the signal of every voxel, which gives a better signal to noise ratio and hence allows acquisition of smaller voxels with still sufficient signal each. To speed up the time consuming 3D acquisition a bit it is possible to divide the whole volume into smaller sections called slabs. For that purpose a slice selection gradient with low amplitude is applied during the excitation RF-pulse. (4,5,6)

2.4 Spoiling

Spoiling is a method to destroy the residual transverse magnetization M_{xy} after an RF-excitation and preventing it from contributing to the signal from the following RF-excitation. This is desireable either for contrast variations or after frequency selective excitation for signal saturation. Spoiling can be achieved by either a gradient, so called gradient spoiling, or by phase modulation of the RF-excitation pulses, called RF-spoiling. In gradient spoiling one to three gradients are activated before the next excitation. The gradient splits the components of the magnetization vector in the same plane that contains the gradient direction. This is called de-phasing. A splitting of the components over a whole turn in this plane is called a 2π-de-phasing. In RF-spoiling the phase of the RF-excitation pulse in the rotating transversal magnetic field is varied between each excitation pulse. This prevents the residual transversal magnetization from contributing to a steady state because the residual transversal magnetization will always be flipped back into the longitudinal magnetization from different phases (i.e. direction) resulting in different net magnetizations. For that purpose the phase can be varied randomly. For a more proper and continuously good result a quadratic phase cycling can be used:

$$\phi_j = \phi_{j-1} + j\phi_0$$

Equation 2.15

Where ϕ_0 is the initial phase and j the index of the TR.

(5,6)

2.5 Gradient-echo-Sequences/ SSFP

Only in a few MR-sequences the direct relaxing signal of the rotating transversal magnetization is collected. This signal is called the free-induction decay (FID). In the majority of the sequences an echo is generated to get a more coherent and stronger signal.

There are two methods to achieve an echo: spin-echo pulse sequence and gradient-echo pulse sequence. Both have in common that a pre-phasing gradient is applied in the readout direction (same as frequency encoding direction) after the RF-excitation. In spin-echo sequences a 180° pulse is given after that to produce an echo. In gradient-echo sequences only a readout gradient in the opposite direction is applied after the pre-phasing gradient. The moment of the pre-phasing gradient corresponds to half of the readout gradient. In that way initial pre-phasing and later re-phasing produce a gradient echo. The echo is located at the middle of the read-out gradient (corresponds to the frequency encoding gradient). The time between the RF-excitation and the echo is called the echo-time (TE) and has the dimension *ms*. This procedure is repeated several times for the read out of a line in the k-space. The time between every repetition is called the repetition time (TR) with the dimension *ms*. A readout matrix of 256 x 256 has 256 TR's in each k-space line. The gradient-echo sequences can be divided into spoiled and refocused sequences. The FLASH and so even the IDEA-FLASH sequence is a spoiled gradient echo sequence. In those sequences the residual transversal magnetization M_{xy} is spoiled by a spoiler gradient at the end of the TR and a quadratic increase of the phase of the RF-excitation pulse between the TR's. In unspoiled, i.e. steady-state free precession sequences (SSFP), the residual transversal magnetization M_{xy} is refocused and after several TR´s M_z and M_{xy} are constant at the same stages in the different TR's, the so called steady state. A special sequence of this group is the balanced SSFP sequence, which means that all gradients are balanced in that way, that the net moment of all gradients for each direction is zero over a TR. This sequence has a superior signal to noise ratio and it is fast, which makes it a preferred sequence in cardiac imaging. At the Siemens scanner the balanced SSFP sequence is called TrueFisp. The echo of the balanced SSFP sequence is located at the middle of the TR, i.e. TR = TE / 2. It takes about 40-50 TR's to reach the steady state. This can be shortened down by sending an α /2-pulse (a pulse with half the flip angle α of the excitation RF-pulse) at the time of TR/2 before the first RF-excitation pulse (α -pulse) is applied. Spins with on-resonance frequency will immediately reach the steady state, while off-resonant spins will reach it in 10-15 pulses. Once the steady state is reached the magnetization vector oscillates between the angle $+\alpha/2$ and $-\alpha/2$. The phase of the α-pulse is increased linearly from TR to TR with this oscillation. (4,5,10)

2.6 Eddy current artefacts

When a varying magnetic flux flows in a conductor an induced electromagnetic field will occur. This induced electromagnetic field itself will produce smaller local currents in conducting material. These currents are called eddy currents. In the MR-scanner the gradient coils produce eddy currents in the conducting material inside the main coil. These eddy currents produce a magnetic field, which is opposite to the field of the gradient coils. This reduces the net gradient field, which results in artefacts in the image reconstruction, where a reverse Fourier transform is calculated with the gradient produced from the coil and not the net gradient and will place the signal at a wrong location in the image space. To reduce eddy currents large gradient jumps and high slew rates should be avoided, which unfortunately isn't an option for a fast sequence as a balanced SSFP sequence. (6,11)

2.7 Pairing

Pairing is a method developed by Bieri, Markl and Scheffler (1) to reduce eddy current artefacts in balanced SSFP sequences. Initially it was developed for unconventional k-space acquisition paths (trajectories). The theory is based on that the balanced SSFP sequence actually has two steady states: one at the magnetization vector at + $\alpha/2$ and the other one at - $\alpha/2$. The magnetization vector is oscillating in-between these two steady states from TR to TR. If similar gradient actions are carried out in pairs, the eddy currents will cancel each other in one pair caused by the same amount but opposite direction due to the opposite path between the two steady states. Larger gradient variations between those pairs are possible. This can also be used for any other action with large gradient activities intermitted in the acquisition as long as the action is carried out twice, i.e. in one pair. Even a slighter extension of the TR in the pairs should be possible due to the opposite path. (1,12,13)

2.8 SAR

A RF-pulse transfers energy to biological tissue, which results in a heating of the tissue. To avoid damage of the tissue and the patient the amount of energy transfer is by law restricted. This energy transfer is measured by the specific absorption rate (SAR), with the dimension *W/kg*. At field strengths used in clinical MRI scanners the SAR is proportional to the RF-bandwidth Δf and the Lamor frequency or hence the field strength B_0 squared and also the flip angle α squared. This gives following relation:

$$SAR \propto B_0^2 \alpha^2 \Delta f$$

Equation 2.16

It is noticed that the energy is transferred to the whole body in the scanner and not only to the area where the spins are resonant. The additional energy amount transferred to the resonant spins is, compared to the thermal transfer, negligibly small. (5)

3 Programming Task

Due to the fact that the code of the IDEA-FLASH is classified as confidential from Siemens no code is published in this thesis. Instead the results with sequence diagrams from the IDEA POET simulator in version VA15 are shown. The challenge of the programming was not just the programming itself. Some of the problems could only be solved by trial and error strategies caused by the fact that the IDEA manual (14) doesn't provide complete explanations for structures in the programming environment or even interfaces in the lower levels.

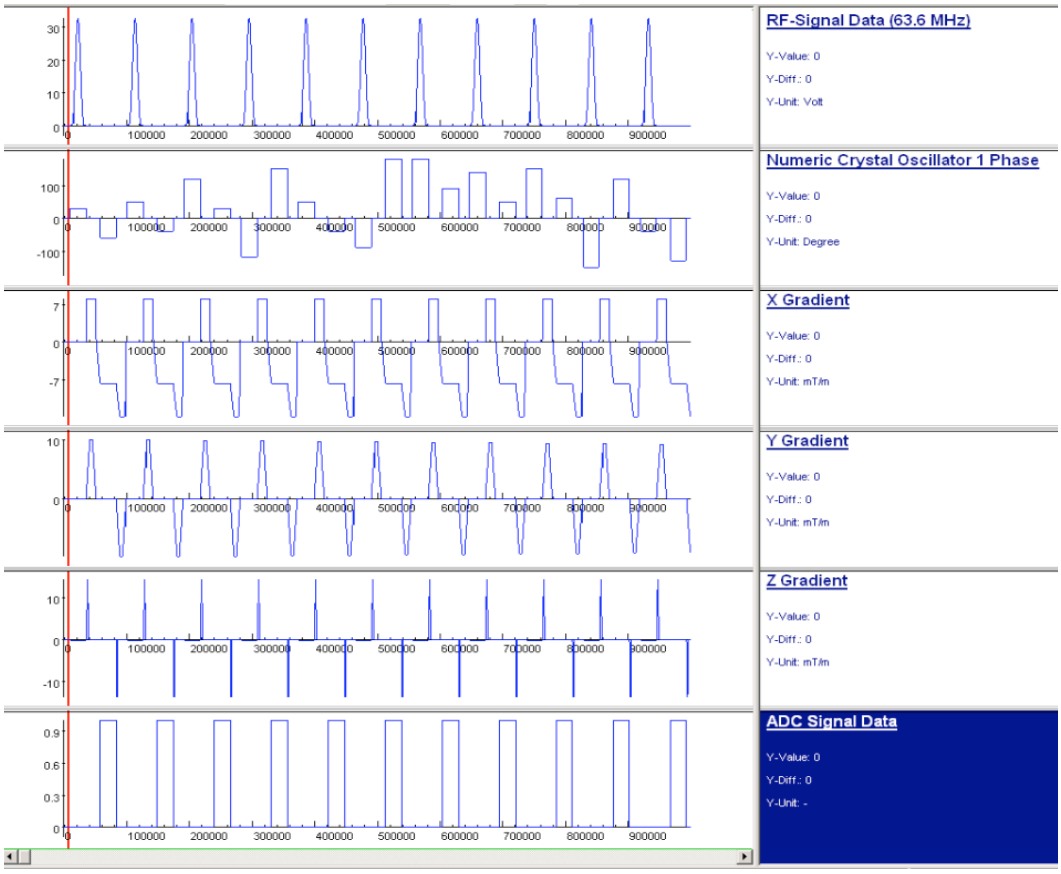

Figure 3.1: IDEA-FLASH sequence diagram from the IDEA POET simulator.

The base for the programming was the IDEA-FLASH, which sequence diagram is shown in the simulator image in Figure 3.1. Characteristic for the FLASH is the gradient echo produced from the x-gradient, the gradient spoiling with the x-gradient and the RF-spoiling of the phase.

The first programming steps were to achieve a balanced SSFP-sequence. For that purpose the gradients over one TR had to be balanced, i.e. the net of all three gradients had to be zero. The phase increase had to be linear and an initial RF-pulse of $\alpha/2$ had to be given TR/2 *ms* in front of the first α-pulse. An image from the simulator is shown in Figure 3.2.

Figure 3.2: Self programmed balanced SSFP sequence diagram from the IDEA POET simulator.

After comparing the self programmed balanced SSFP sequence with the Siemens product sequence TrueFISP without major differences in the images, the pairing based fat-saturation was implemented.

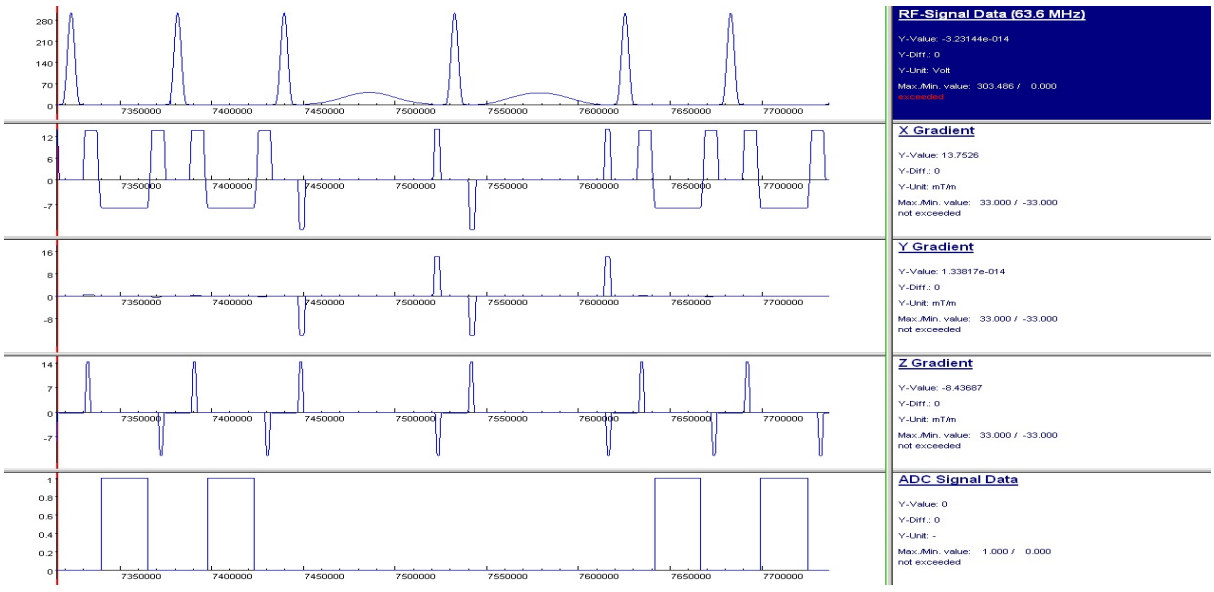

Figure 3.3: Pairing block sequence diagram from the IDEA POET simulator.

Figure 3.3 shows the pairing block with the fat-saturation pulses in the sequence simulator.

To avoid time-consuming compilation and sequence transfers to the scanner, the most important parameters needed for the evaluation of the sequence were implemented in the user interface at the scanner as a special card. For the implementation the script Parameter Map from Maxim Zaitsev (15) was used, which shortens the amount of code lines. The drawback of this script is that it only works for the IDEA-sequence and not for the product sequence.

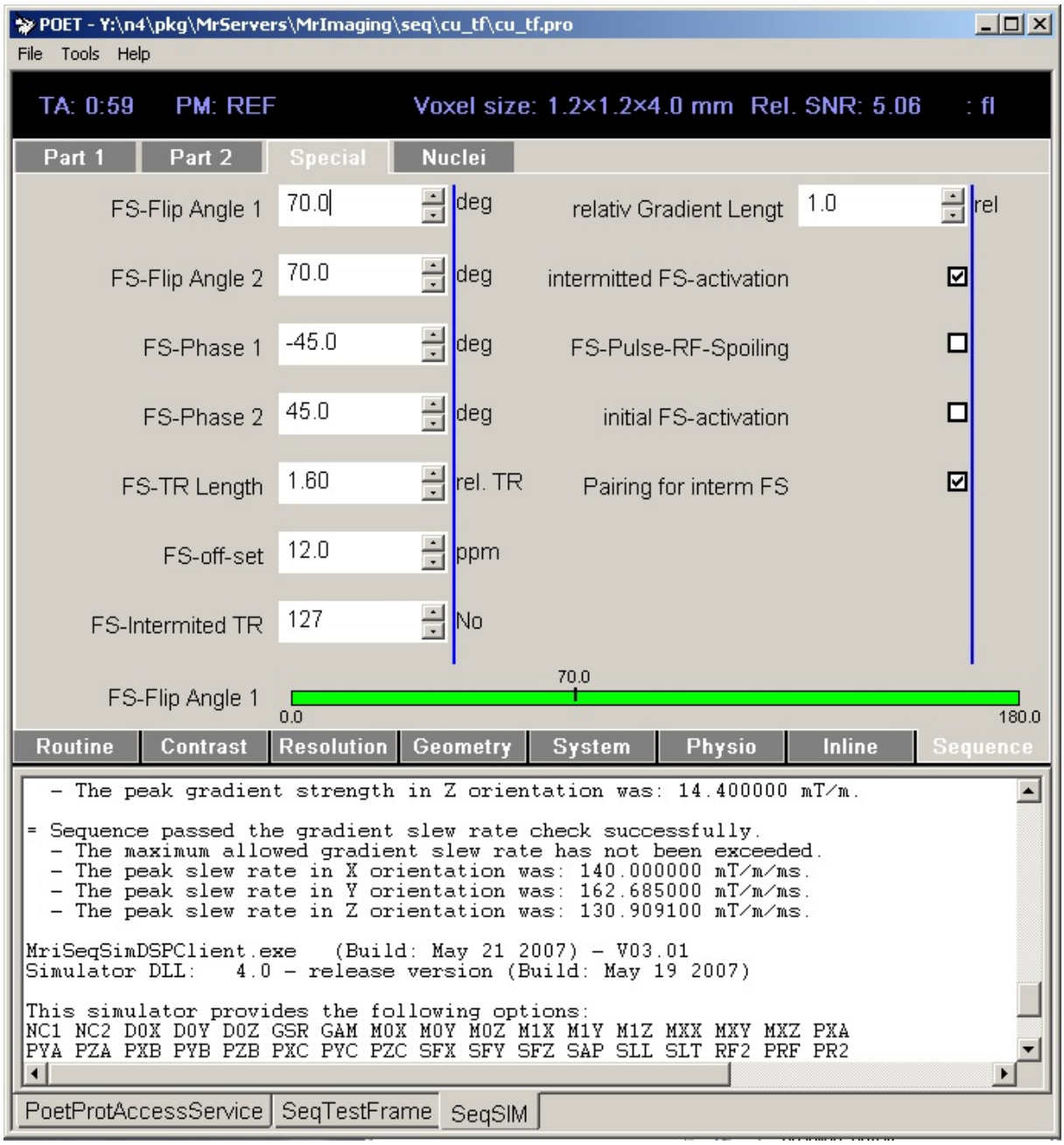

Figure 3.4: Special card at the scanner user interface for adjustments of the pairing fat-saturation parameters

Figure 3.4 shows a screen print of the special card. Followed are the explanations for the different parameters given:

FS-Flip Angle 1 and 2: Adjustment of the flip angle for the fat-saturation pulse in the first and second TR in the pairing block.

FS-Phase 1 and 2: Adjustment of the initial phase for the fat-saturation pulse in the first and second TR in the pairing block

FS-TR-length: Factor by that the images acquisition TR is multiplied to get the FS-TR-length.

FS-off-set: Frequency offset of the fat-saturation pulse from the water-proton frequency in ppm.

FS-intermitted TR: number of TR before the fat-saturation block is played out, in the sequence version where multiple pairing blocks in every k-space line are played out this is the number of TR's in between the fat-saturation blocks.

Relative gradient length: Adjustment for the spoiler gradient moment, where 1.0 corresponds to a moment of 2π.

Intermitted FS-activation: on/off for the pairing block

Initial-FS: If activated a fat-saturation pulse is played out before the image acquisition starts

FS-pulse-RF-spoiling: on/off

Pairing for interm FS: If on the fat-saturation block has a pairing configuration with 2 fat-saturation TR's.

4 Method and Setup

After programming the sequence in C++ the sequence files were compiled and tested in the simulation in the IDEA-sequence development tool provided from Siemens on a separate workstation. On the simulator the sequence was tested with different parameters. When the simulator showed a correct sequence diagram the files where copied to the scanner. The IDEA-sequence development tool and the scanner were equipped with the software-version VA15. The final sequence has been tested on both a 3T Avanto and 1.5T Espree Siemens clinical scanner.

Figure 4.1: The Siemens MAGNETOM Espree 1.5 Tesla clinical MR-scanner used for the optimization of the sequence.

For the optimization only the Siemens Espree 1.5T medical scanner – shown in Figure 4.1 - was used, so all results of this thesis are based on the measurement at 1.5T. The main difference to the 3T Avanto Siemens scanner is a higher offset frequency, which would result in a more frequency selective fat-saturation pulse at the same pulse-length at the 3T-system.

As a measuring object for the optimization, a Siemens standard water-phantom bottle and two smaller bottles filled with commercial sunflower oil, purchased in a food store, were used. The three bottles are shown in Figure 4.2

Figure 4.2: Measuring object for the optimization were a Siemens standard water phantom and two smaller bottles filled with sunflower oil.

To get the best signal to noise ratio a Siemens 12-channel head-coil was chosen for the examination. The objects were placed approximately symmetric in the centre of the head coil, which is shown in Figure 4.3. Once the optimal parameters where determined on the phantom-object a series of a knee from a healthy volunteer was acquired. For this purpose an 8-chanel knee-coil from Invivo (Invivo Corporation, Gainsville, FL, USA) was used.

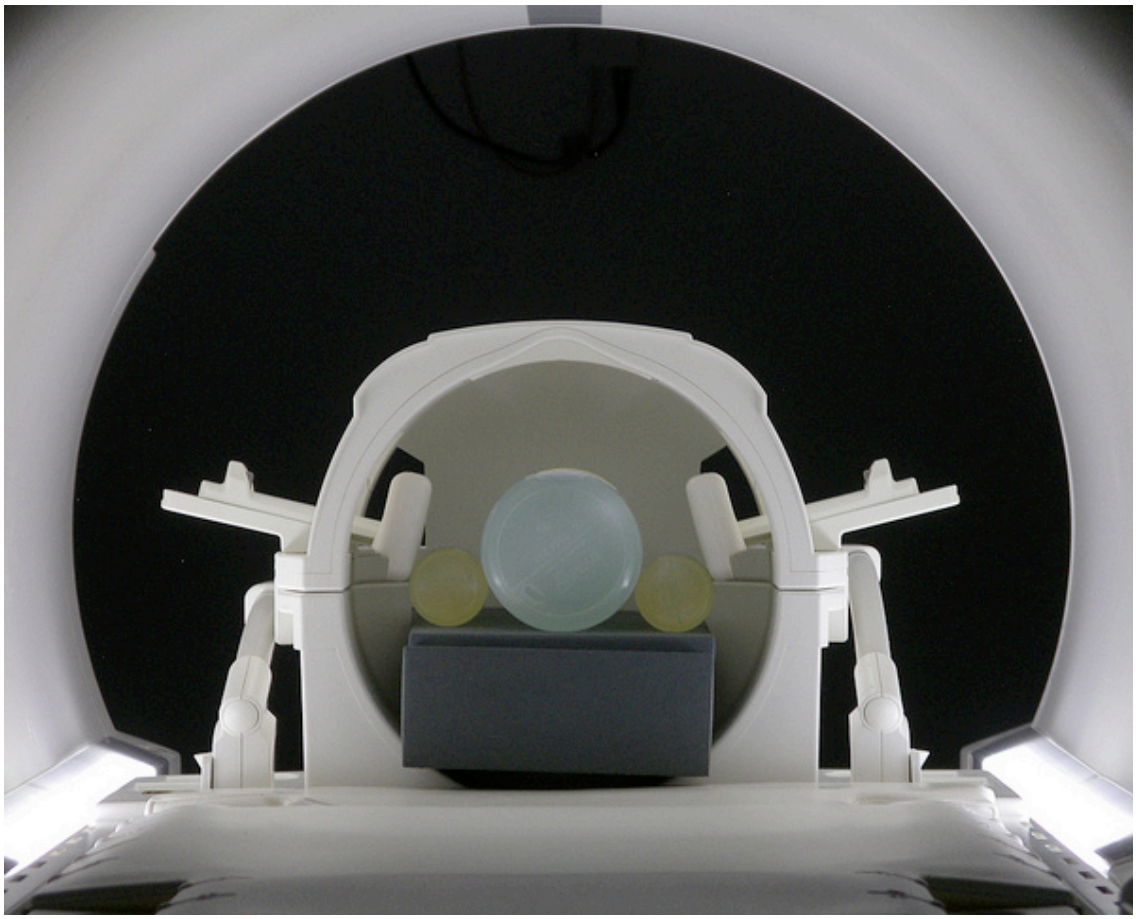

Figure 4.3 Positioning of the phantom objects symmetrically at the centre in the head coil in the scanner.

5 Results

The results of the measurements are presented as images. It is a copy of the Dicom-Image the scanner has reconstructed after the acquisition.

5.1 IDEA-FLASH

For comparison a acquisition with the IDEA-FLASH-sequence – which is the unmodified base-sequence - was performed both without and with fat suppression.

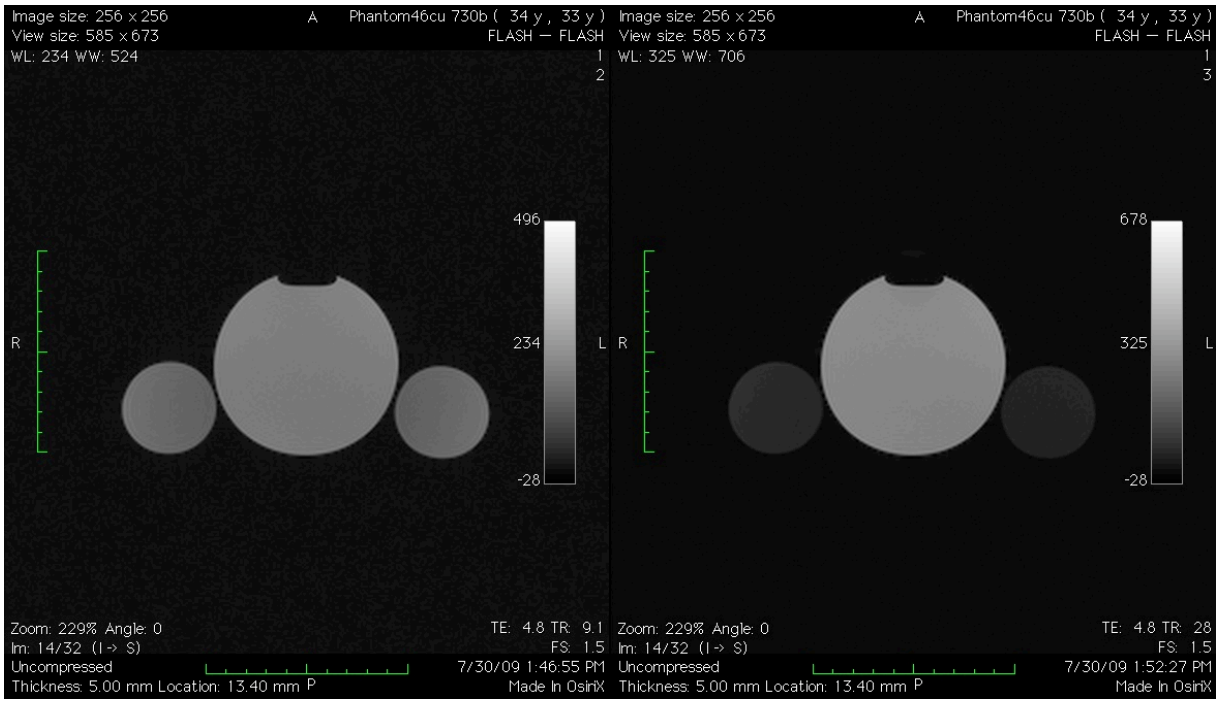

Figure 5.1: 3D-FLASH-acquisition on the left side without fat saturation and to right with fat saturation with windowing used in medical imaging

The result of the 3D-FLASH-acquisition is shown in Figure 5.1, which shows a sufficient fat suppression where the oil-filled bottles only are slightly visible in window level settings comparable to medical imaging. Nevertheless, in some slices there occur artefacts already visible in windowing used for medical imaging.

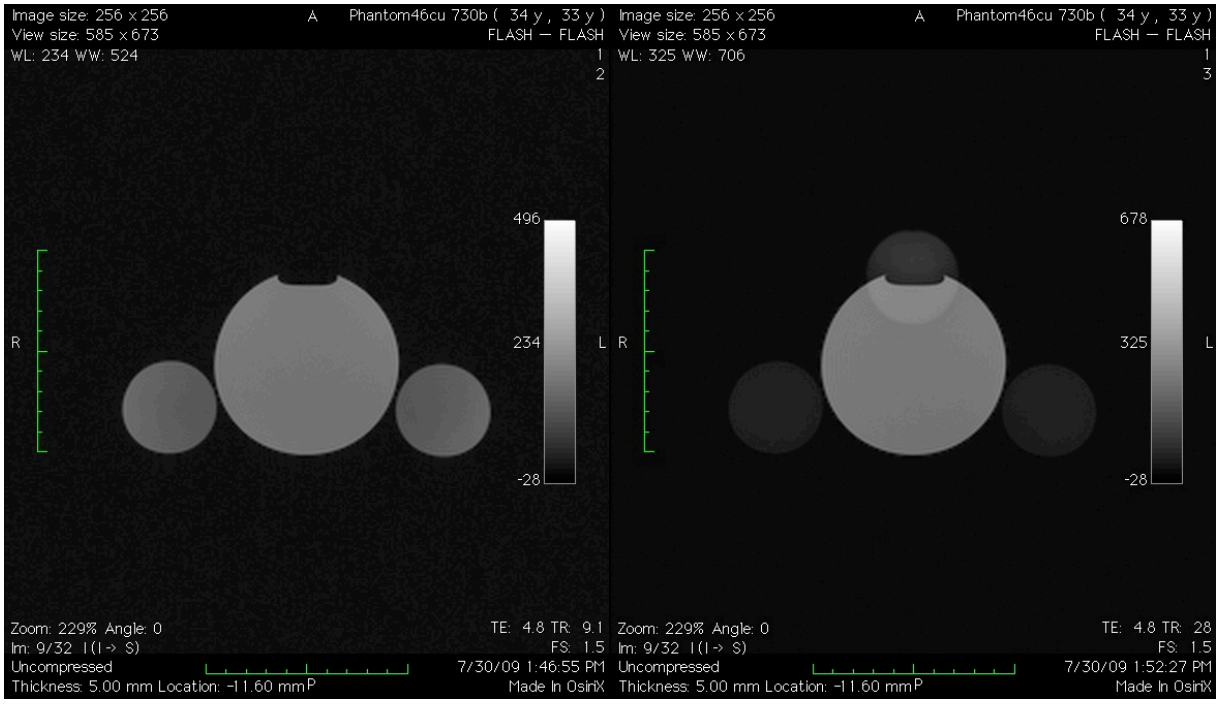

Figure 5.2: A slice from the midrange of the 3D-block in the FLASH-acquisition, on the left side without and on the right side with fat saturation

Figure 5.2 shows a slice from the midrange of the 3D-block of the FLASH-acquisition with medically used window levels. In the fat saturated image on the right side a

ghosting artefact from an oil bottle is visible at the top of the water bottle. The artefact occurs more obviously when the windowing is changed to enhance the contrast in the air space surrounding the object, i.e. visualization of the noise and artefacts. This windowing is not used for medical imaging but sufficient to obtain technical information through artefacts.

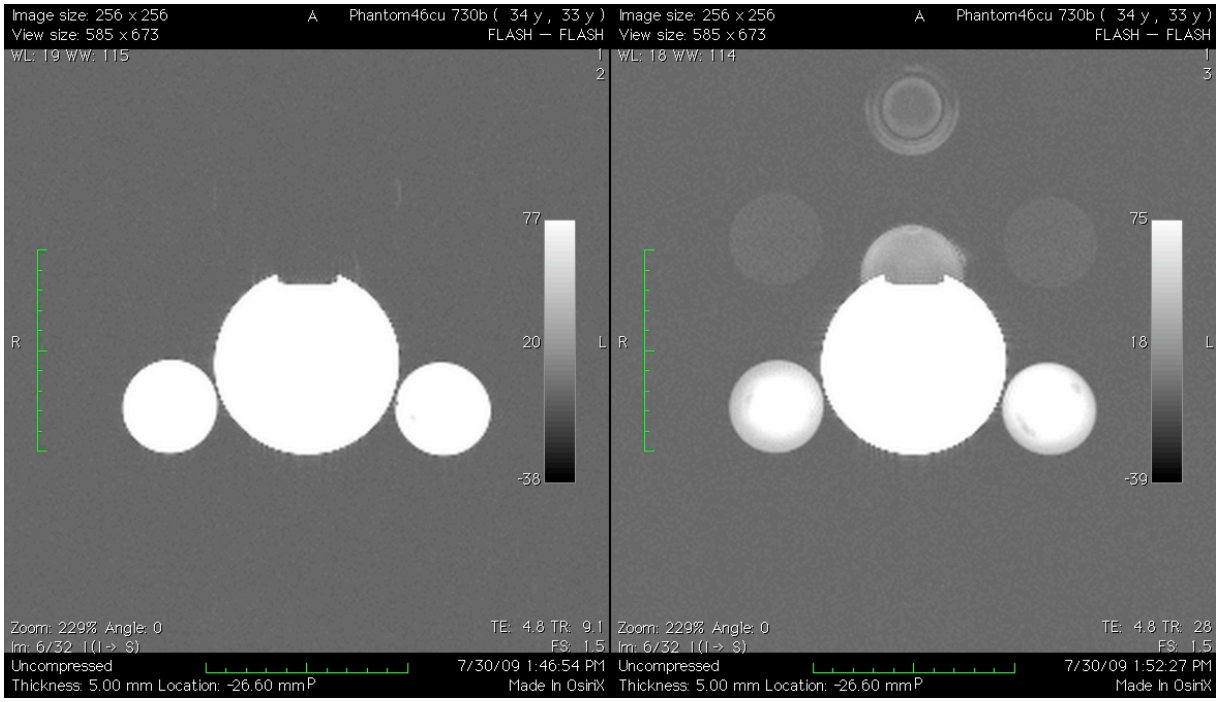

Figure 5.3: Same midrange slice as in Figure 4.2 from a 3D-FLASH-acquisition, with windowing for contrast enhancing the air space and noise, to the left without and to the right with fat saturation

As well as the fact that the artefact on top of the water bottle is more obvious by the windowing in Figure 5.3 it also uncovers 3 additional ghost artefacts from the oil bottles. These artefacts are not caused by folding, because the oil bottles were totally covered in the 3D-volume – even folding of the water bottle was sufficiently suppressed by a slice oversampling on 37.5%. Most likely the artefacts are caused by insufficient spoiling of the fat signal, which might be reintroduced to the k-space by the unselective α-pulse.

5.2 Product TruFisp

Whilst the IDEA-FLASH-sequence is the base for the derived balanced SSFP-sequence in this project, the image contrast is not comparable between the spoiled and balanced sequence. Due to this, some series were acquired with the product SSFP-sequence, the TrueFisp-sequence, to be able to compare the result of the self-programmed version.

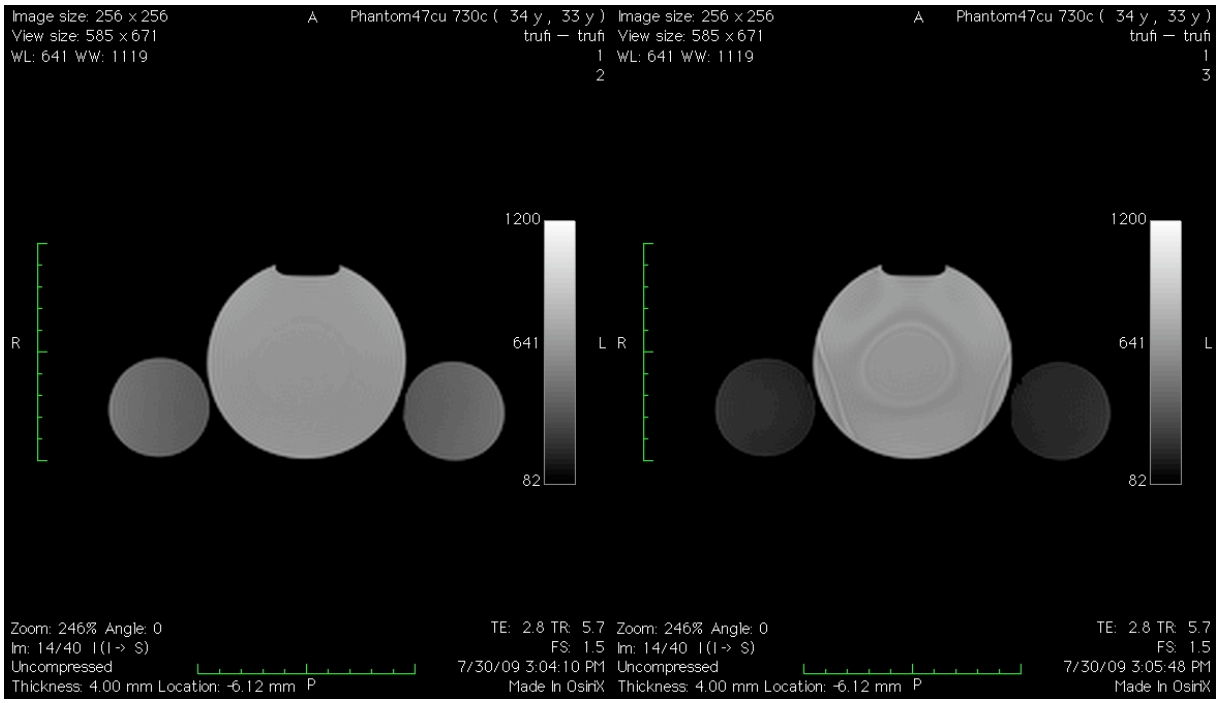

Figure 5.4 Product 3D-TrueFisp sequence with windowing used in medical imaging, to the left without and to the right with fat saturation

Figure 5.4 shows the images of the Siemens product TrueFisp-sequence without and with fat saturation in windowing used for medical imaging. Both images show the TrueFisp typical ringing-artefact, which is shown in a detail image in Figure 5.5.

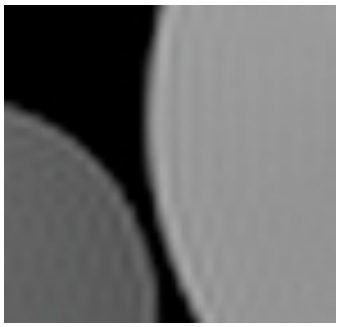

Figure 5.5 Detail image with Ringing-artefact from product TrueFisp-sequence in Figure 5.4

Due to the fat saturation in the product-TrueFisp-sequence, some artefacts occur in the water bottle. Nevertheless, in images levelled with typical medical windowing, no artefacts outside the objects are visible.

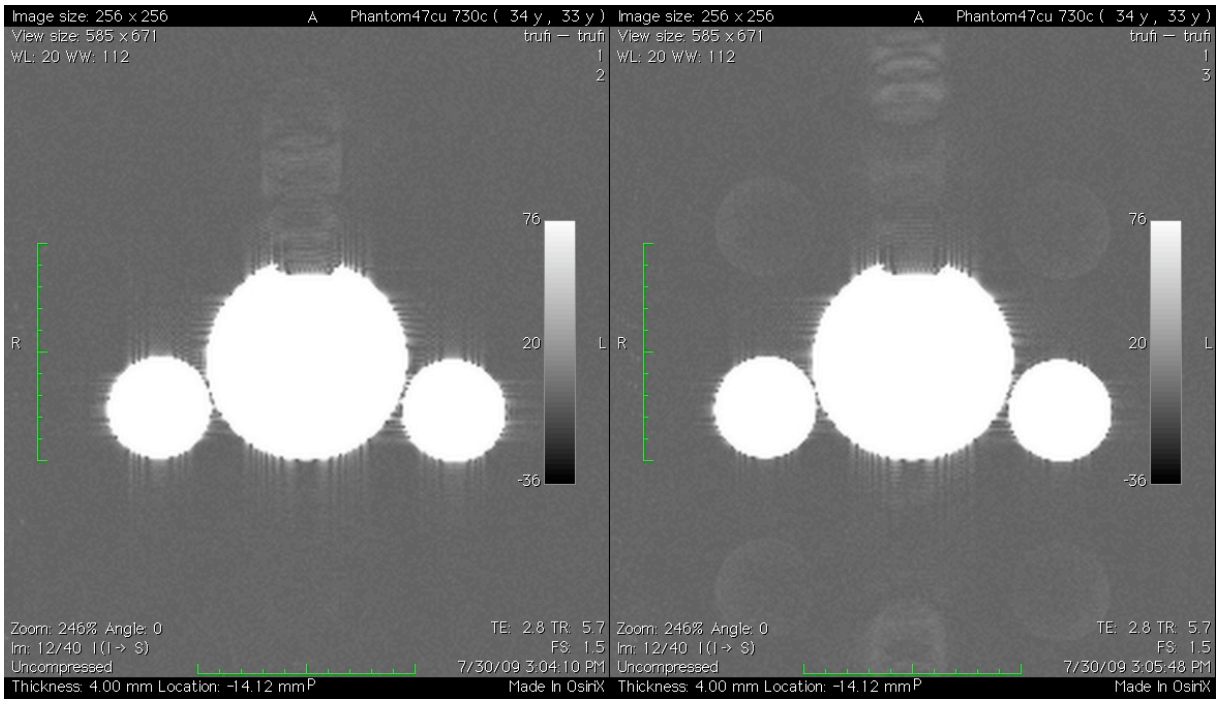

Figure 5.6: Midrange slice from the same product 3D-TrueFisp-acquisition as Figure 5.4, with windowing for contrast enhancing the air space and noise, to the left without and to the right with fat saturation

Figure 5.6 shows the same acquisition as in Figure 5.4 with the product 3D-TrueFisp-sequence but window-levelled for contrast enhancing the airspace. It reveals only slight artefacts, which are not compromising the medical imaging.

5.3 Balanced SSFP with constant k-space line direction vs. alternating direction

During the programming task the first step was to achieve a proper and stable balanced SSFP sequence.

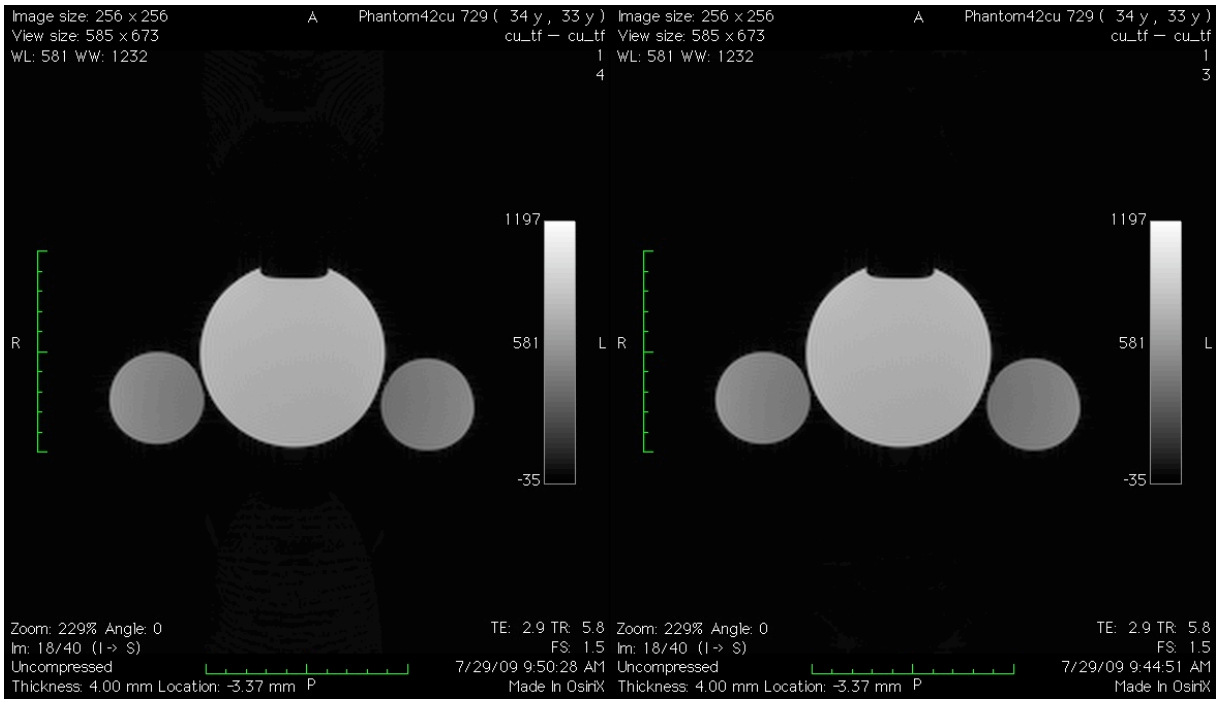

Figure 5.7: Acquisition with programmed TrueFisp outgoing from the IDEA-FLASH, to the left with constant line direction and to the right with meandering k-space acquisition

Figure 5.7 shows the result of the self-programmed TrueFisp sequence started from the IDEA-FLASH as a base for the programming task. The image on the left is acquired with constant k-space line direction whilst the image to the right is acquired with meandering thru the k-space to reduce higher gradient variations and hence eddy currents. Comparing those images to the product TruFisp-image Figure 5.4 to the left, there is no difference in the image levelled like medical images. All three images have the TrueFisp typical ringing artefact and same contrast. There is even no difference at that window level between the two different k-space-acquisition-paths.

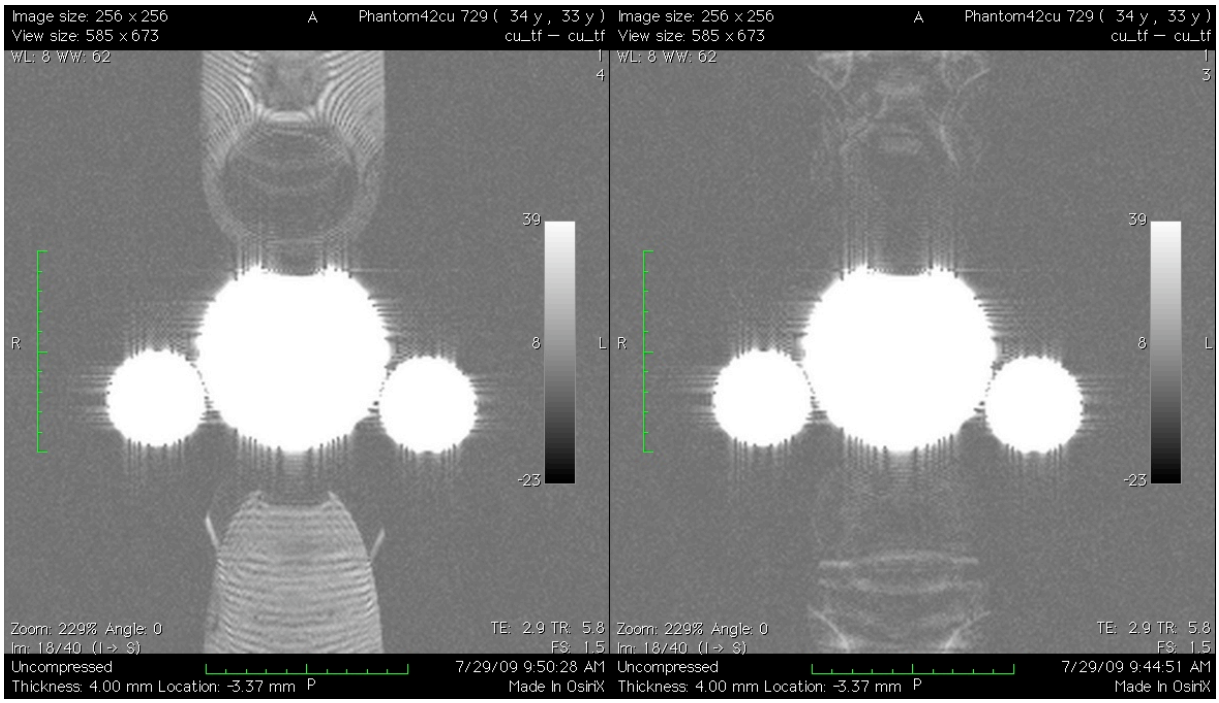

Figure 5.8: Same acquisition with self-programmed TrueFisp outgoing from the IDEA-FLASH as in Figure 5.7 but window leveled to contrast enhance the air space and noise, to the left with constant line direction and to the right with meandering k-space acquisition

Nevertheless the same images levelled for contrast enhance the air space and noise in Figure 5.8 reveal more artefacts when the k-space is acquired in constant line direction. The image to the right with a meander path has a comparable artefact level to the product sequence in Figure 5.6 to the left.

5.4 Optimal frequency offset in ppm from the water-frequency

As mentioned in the theory chapter the fat-attached protons have a slightly different frequency than free water protons with a frequency offset of 3.5 ppm below the water-resonance frequency. Due to the time-bandwidth product for a Gaussian pulse, which is defined as $\Delta t \cdot \Delta f \approx 2.8$, a pulse of 1ms would have a bandwidth of 2,800 Hz. If the centre frequency of the fat-saturation pulse with duration of 1ms is localized at 3 ppm of resonant to the water the pulse will still overlap the water resonance frequency by nearly 1.200 Hz at a 1.5 Tesla scanner. This would cause an unwanted signal loss or saturation of the water-protons. To avoid water signal-loss either the pulse-length must be increased or the offset frequency of the pulse must be increased.

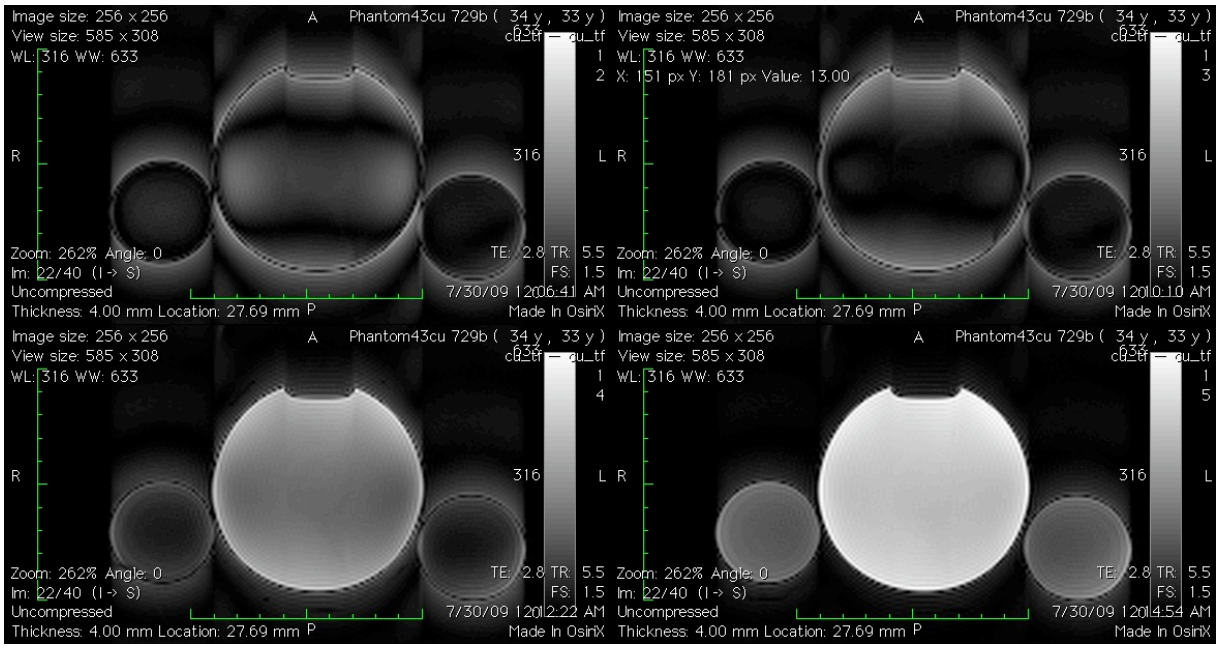

Figure 5.9 variation of the off-set frequency of the fat-saturation pulse from 6ppm at the left on top increasing by 3 ppm to 15 ppm to the right at the bottom

Figure 5.9 demonstrates the results of the variation of the offset frequency whilst the pulse length is fixed to constant duration. The best compromise between sufficient fat-saturation and still acceptable signal-loss in the water is at 12 ppm. At 15 ppm the water-signal loss is not visible but even the fat-saturation is insufficient, hence at 6 and 9 ppm the water signal is suppressed nearly in the same range as the fat signal.

5.5 Location of the intermitted fat-saturation in the k-space-line

The localization of the intermitted fat-saturation during the acquisition of the k-space is of importance. One of the first approaches was to play the fat-saturation TR-block out after a fixed number of acquisition TRs in every k-space line.

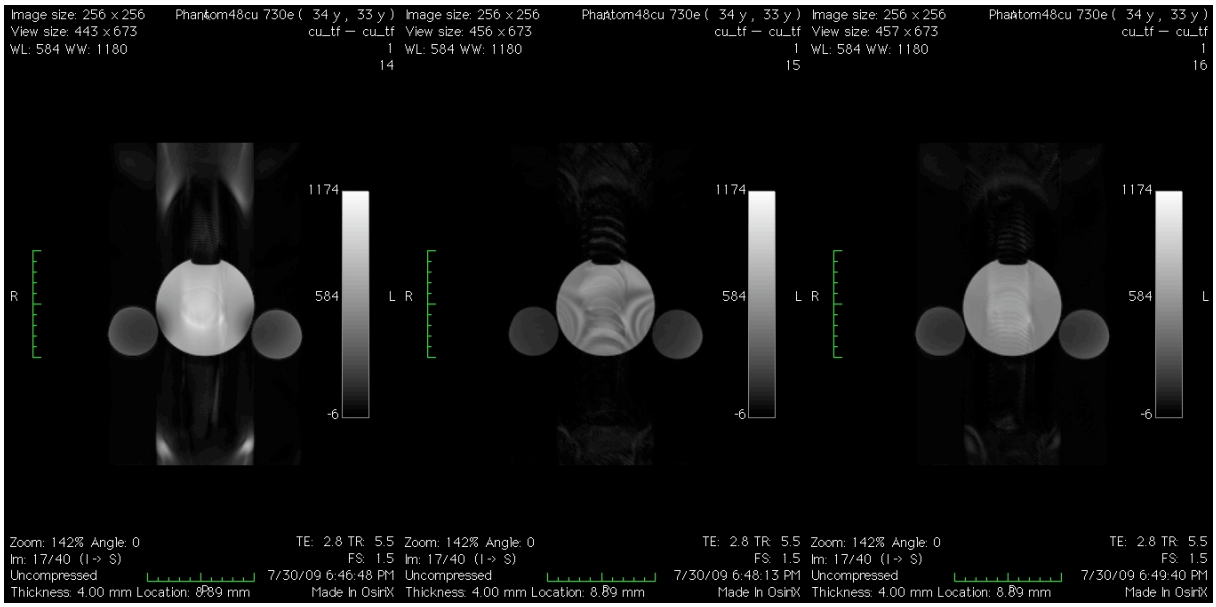

Figure 5.10 different fat-saturation schemes, hence to the distance between the fat-saturation blocks in every k-space lines, played out after every 20 TRs (on the left), 30 TRs and 62 TRs (to the right). Images at a 256x256 matrix.

The results of multiple fat-saturation blocks per k-space-line are demonstrated in Figure 5.10, where it is shown that increasing the number of intermitted fat-saturation blocks per k-space line causes a progression of artefacts. The level of fat-saturation seems only to be affected slightly. This result was the reason for an implementation of a scheme of only one fat-saturation pulse per k-space line.

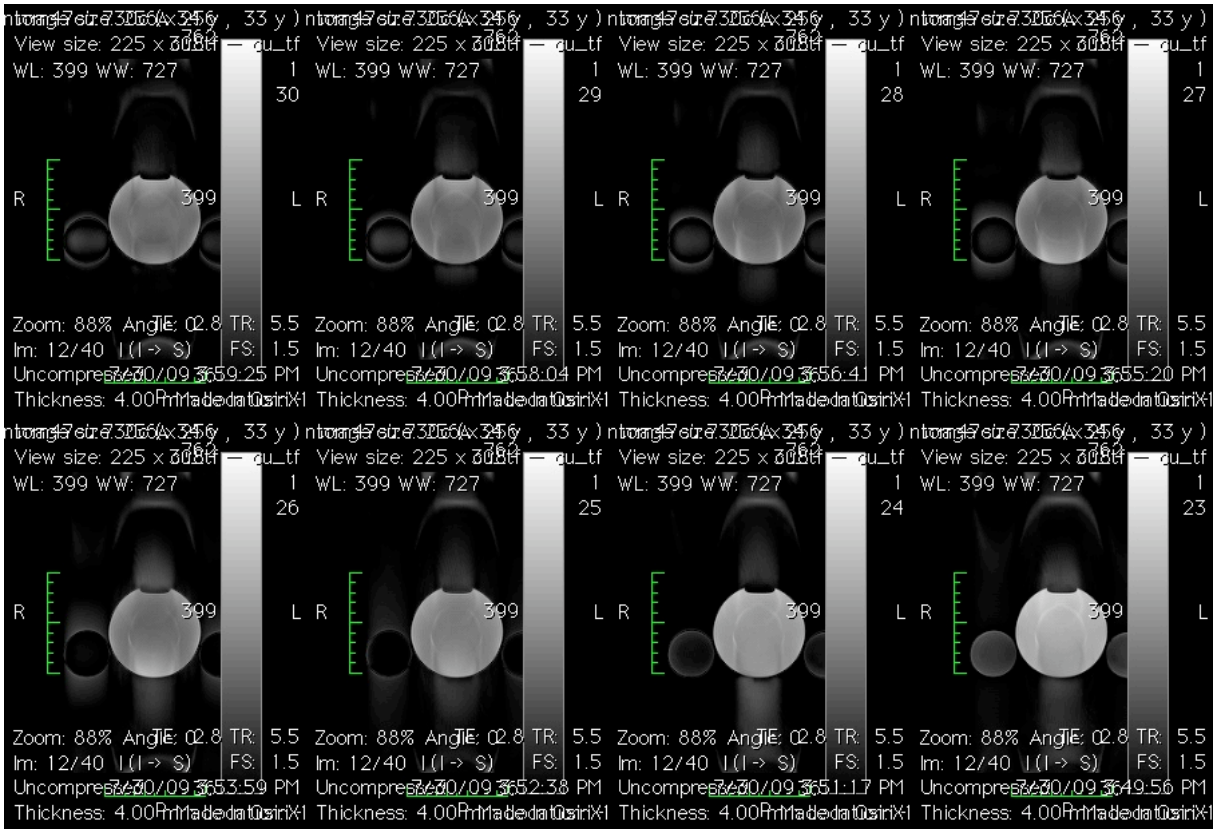

Figure 5.11 Fat-saturation scheme with only one saturation block per k-space line with localization after the 122nd TR (at top left) increasing by 1 to the 129th (at bottom right) at a 256 matrix

In Figure 5.11 are the results for a single fat-saturation block at different localizations at the k-space shown. The acquisition matrix is 256 x 256, hence the centre line is at the position 128. The series shows the best fat-saturation result for the acquisition with a fat-saturation played out after the 127th TR. While positioned directly after the centreline the effect of the fat-saturation is still acceptable, it rapidly fades if positioned only one TR later. It is recognized from the images that a saturation block nearby but in front of the centre line gives a sufficient suppression of the area of the oil bottle but the contour is still visible with high contrast. This is explained by the fact that the centre of the k-space contains the contrast and the periphery, with the higher frequency components, contains the contour of the image and, in this setup, no suppression is made in the periphery.

5.6 Influences of gradients in the fat-saturation block on image artefacts

The activation of the fat-saturation block with pairing causes some artefacts. As the fat-saturation block contains several different parts, i.e. pulses and gradients, it is uncertain, which component generates most of the artefacts. The α-pulse and the slice-selection gradient are the same as in the image-acquisition-TR and due to that rarely the source for the artefacts. To distinguish the artefact component from the fat-saturation spoiler gradient and the fat-saturation pulse a series with a fat-saturation flip angle of 0° was acquired. In this setup no fat saturation pulse is played out and the time between the de-phase gradients is similar to the fat-saturation pulse duration, which causes in the same fat-saturation block-TR as if the pulse had been played out.

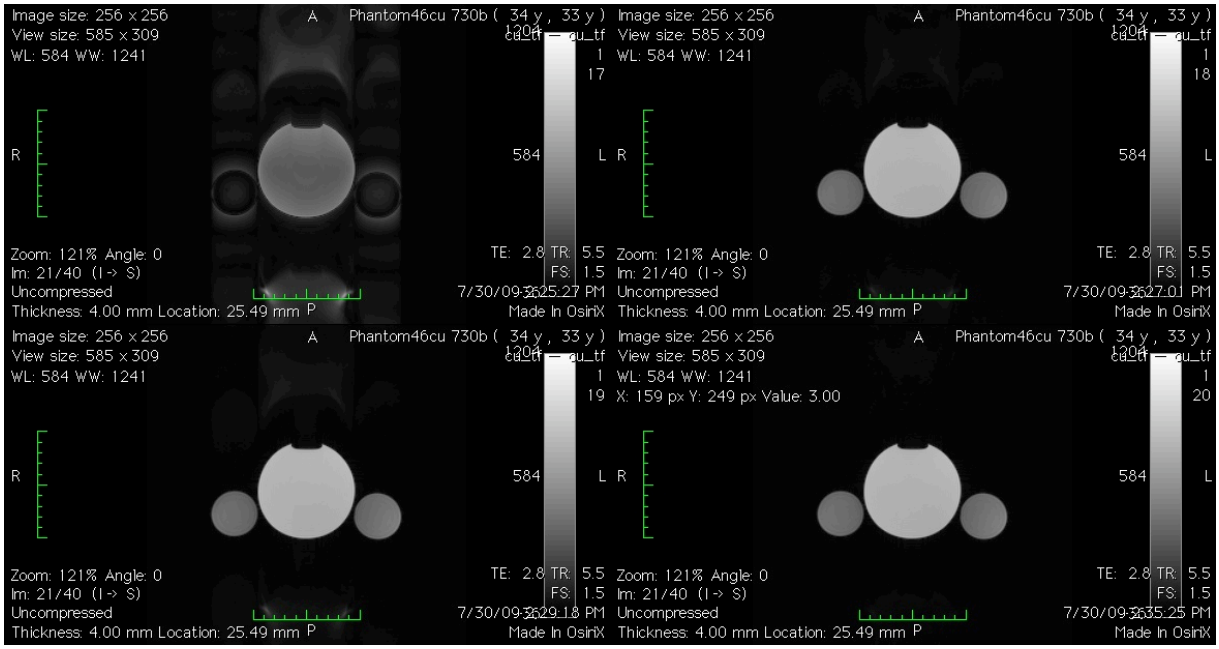

Figure 5.12 top left: fat-saturation with two 90° flip angle and 0.4π-moment de-phase gradient; top right: no fat-saturation pulse (flip angel = 0°) and 0.4π-moment de-phase gradient; bottom left: flip angle = 0° and 1.0π-moment de-phase gradient; bottom right flip angle = 0° and no gradient

As shown in the Figure 5.12 most of the artefacts vanish when the fat-saturation pulse is deactivated. By increasing the moment of the spoiler gradient a slight artefact in top and below the water-phantom occurs. This artefact doesn't affect the image much if it is levelled like medical images.

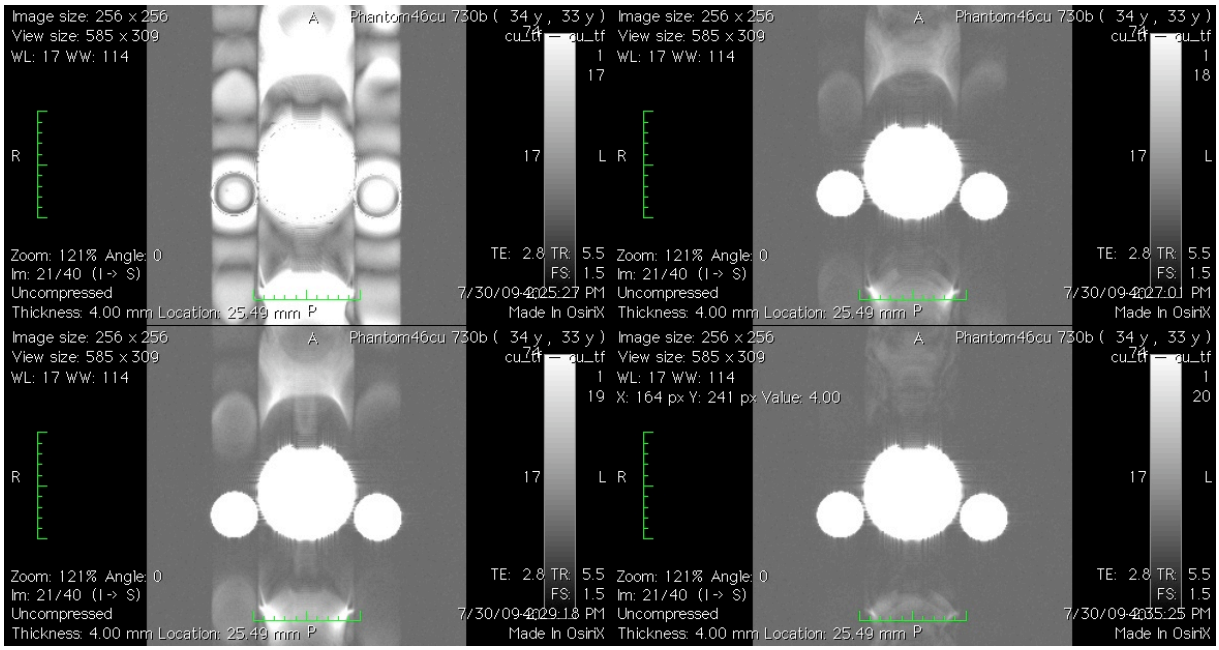

Figure 5.13 Same acquisition as in Figure 5.12 but, window levelled to contrast enhances the air space and noise. Top left: fat-saturation with two 90° flip angle and 0.4π-moment de-phase gradient; top right: no fat-saturation pulse (flip angel = 0°) and 0.4π-moment de-phase gradient; bottom left: flip angle = 0° and 1.0π-moment de-phase gradient; bottom right flip angle = 0° and no gradient

Levelled to contrast enhance the artefacts, as shown in Figure 5.13, the artefacts caused by the de-phase gradients are more obvious. But they are still small compared to the artefacts caused by the fat-saturation pulse. As a remark it should be mentioned that a series with a fat-saturation pulse but no de-phase gradients would not be useful, because the fat-signal would give plenty of artefacts when the fat-signal isn't moved out side the k-space.

5.7 Variation of the spoiler-phase gradient length/moment

Theoretically a spoiler-gradient moment of 1.0*π or higher would be optimal to de-phase the fat signal. But this would cause a broad bandwidth of the fat-saturation pulse if the TR-length of a single fat-saturation block were kept in the range of an image acquisition TR. In this series with variation of the spoiler-gradient length with constant maximal amplitude a compromise between a fat-saturation pulse affecting the water-signal and a suboptimal de-phasing of the fat signal with a fraction still generating a signal in the k-space can be found.

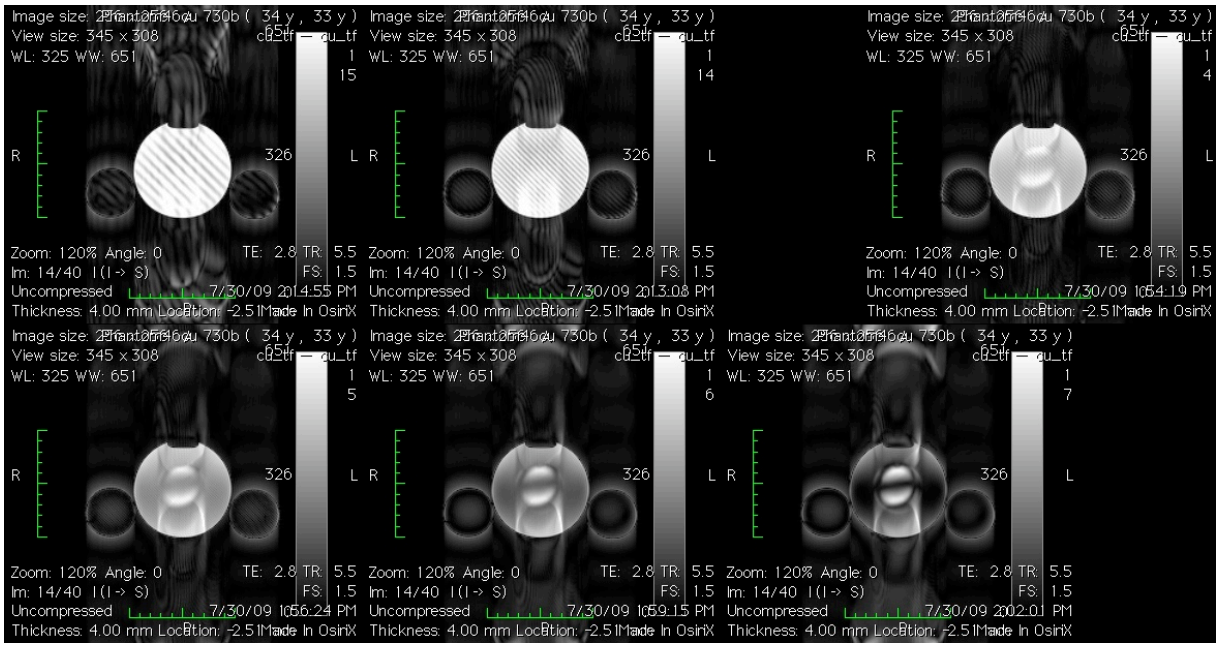

Figure 5.14 Series with increasing the de-phase gradients from 0,1π–moment at top left to 0.6π-moment at bottom right by 0.1π-steps, while the fat-saturation block TR is kept constant.

Figure 5.14 shows a series with increasing de-phase gradient moments while the fat-saturation block length is kept constant. At low moments multiple lines in an angle of 45° occur, which corresponds to a high signal intensity in the k-space on a 45°-axes. By increasing the moment the line-distance decrease (or the line frequency increases) until the signal is outside of the k-space and doesn't generate line-artefacts any more. At higher moments the length of the fat-saturation pulse is reduced and the bandwidth increased. This results in water-signal suppression. From Figure 5.14 the best compromise between de-phasing and water-signal suppression seems to be at a moment of 0.4π.

5.8 RF-spoiling

In the used setup of the fat-saturation block the fat-saturation pulse is given at the same phase. As the fat-saturation lasts for approximately 200ms there would be a risk for an own steady state of the fat-signal if a fat-saturation pulse at the same phase were applied during this interval. Actually, the fat-saturation block is activated once per line in a 256 matrix and a TR of 5.5 ms, resulting in a time of 1408ms between every fat-saturation block. Thus the inter block duration should not cause any steady state in the fat signal. But the fat-saturation block contains in pairing two fat-saturation pulses in a distance of one fat-saturation TR, which in most of the acquired series is between 5,5 – 8ms.

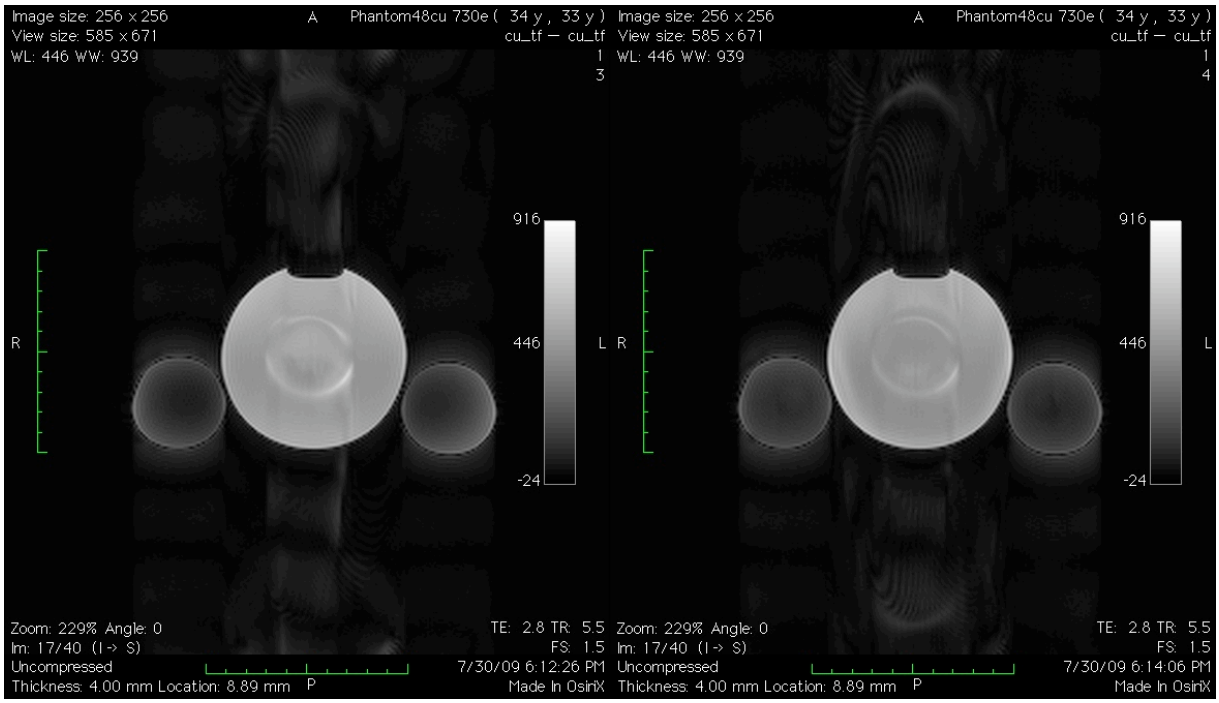

Figure 5.15 Fat-saturated image with standard parameter to the left without RF-spoiling and to the right with RF-spoiling in the fat-saturation block.

Figure 5.15 shows the result of the comparison of none-RF-spoiling and RF-spoiling in the fat-saturation block. There is no visible difference in the images.

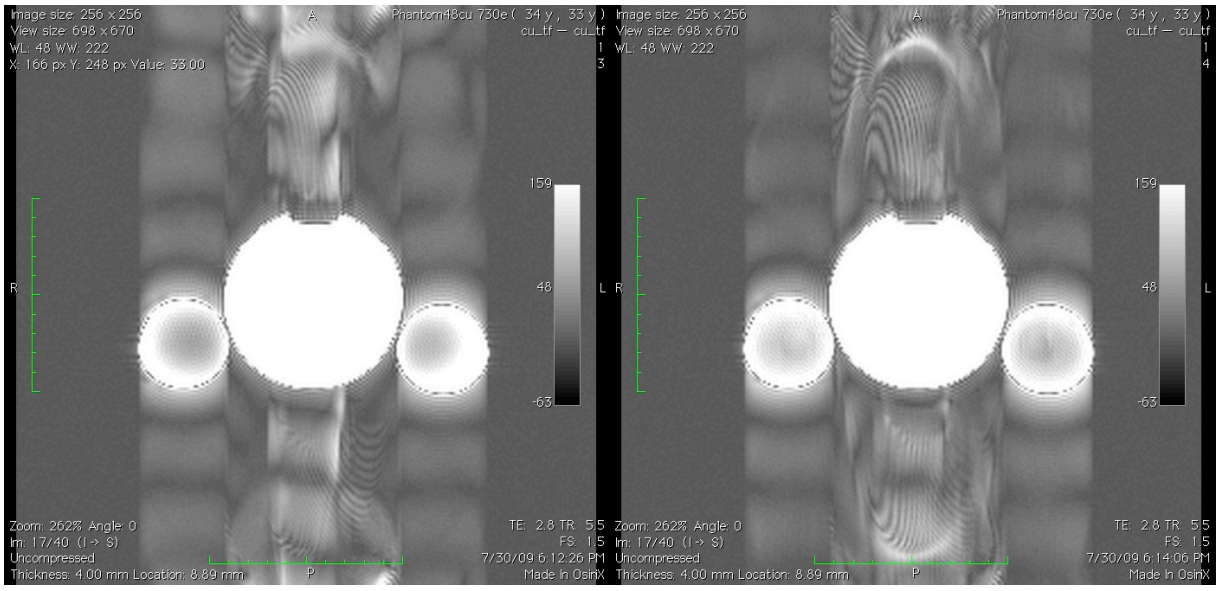

Figure 5.16 Same acquisition as in Figure 5.15 but, window levelled to contrast enhances the air space and noise. Fat-saturated image with standard parameter to the left without RF-spoiling and to the right with RF-spoiling in the fat-saturation block

Even in Figure 5.16 where the images are levelled to a window level for revealing artefacts, there is no difference visible in the images.

5.9 Variation of the TR-length of the fat-saturation block

As mentioned above in the section about the optimal offset frequency, the fat-saturation pulse length should be as long as possible to reduce the bandwidth and hence increase

the selectivity of the fat-saturation pulse. In theory the pairing principle should allow to increase the TR of the fat-saturation block over the image acquisition TR.

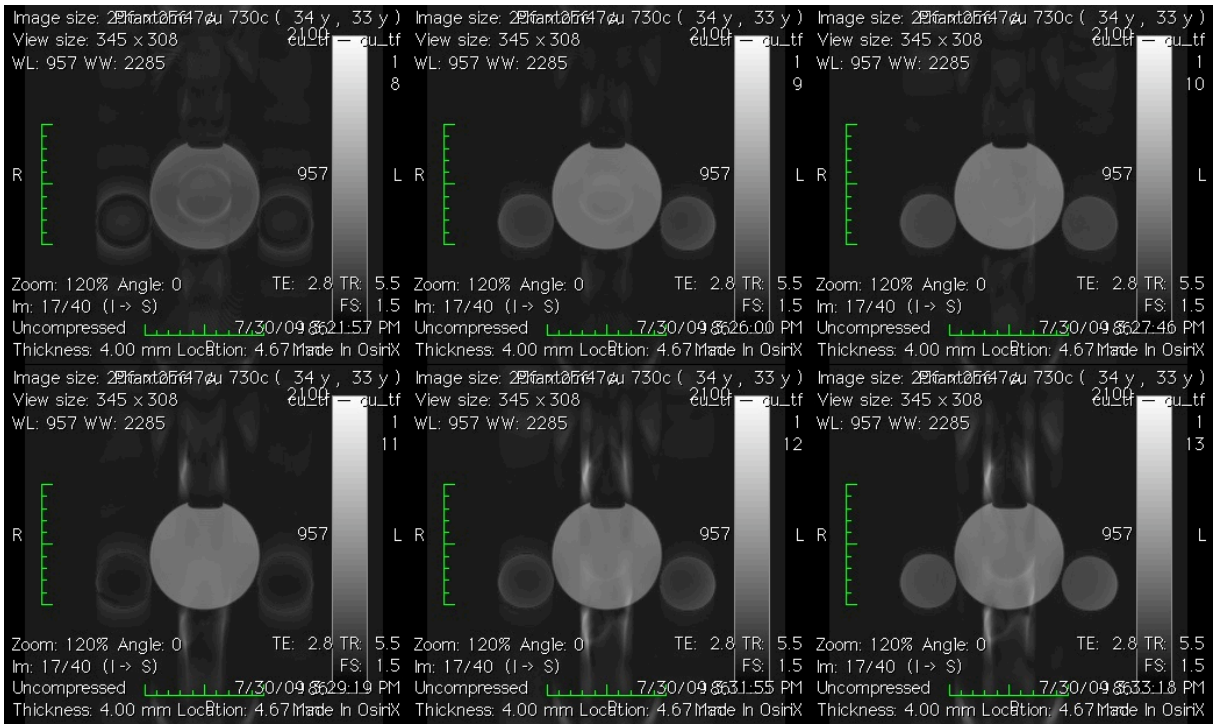

Figure 5.17 Series with increasing the fat-saturation TR from the factor 1.0 of the imaging TR at top left increased by 0.2 to 2.0 at bottom right. The moment of the spoiler gradients kept constant 0,4π, while the fat-saturation pulse duration increases.

The series with variation of the fat-saturation TR by constant kept gradients and hence variation of the fat-saturation pulse in Figure 5.17 shows a variation of the fat-intensity reduction with the highest reduction at a fat-saturation TR-length of 1.0 and 1.6 times the imaging TR-length. The optimum between fat-saturation and none affecting the water signal is in this series at a fat-saturation TR of 1,6 x imaging TR caused by a lower affection off the water signal then at factor 1.0. It is noticed that there is none linear dependency of the fat signal reduction with relative minima and maxima of the fat intensity at different TR-length. Not shown in this series is that by further increasing there will occur another relative minimum in the intensity of the fat signal.

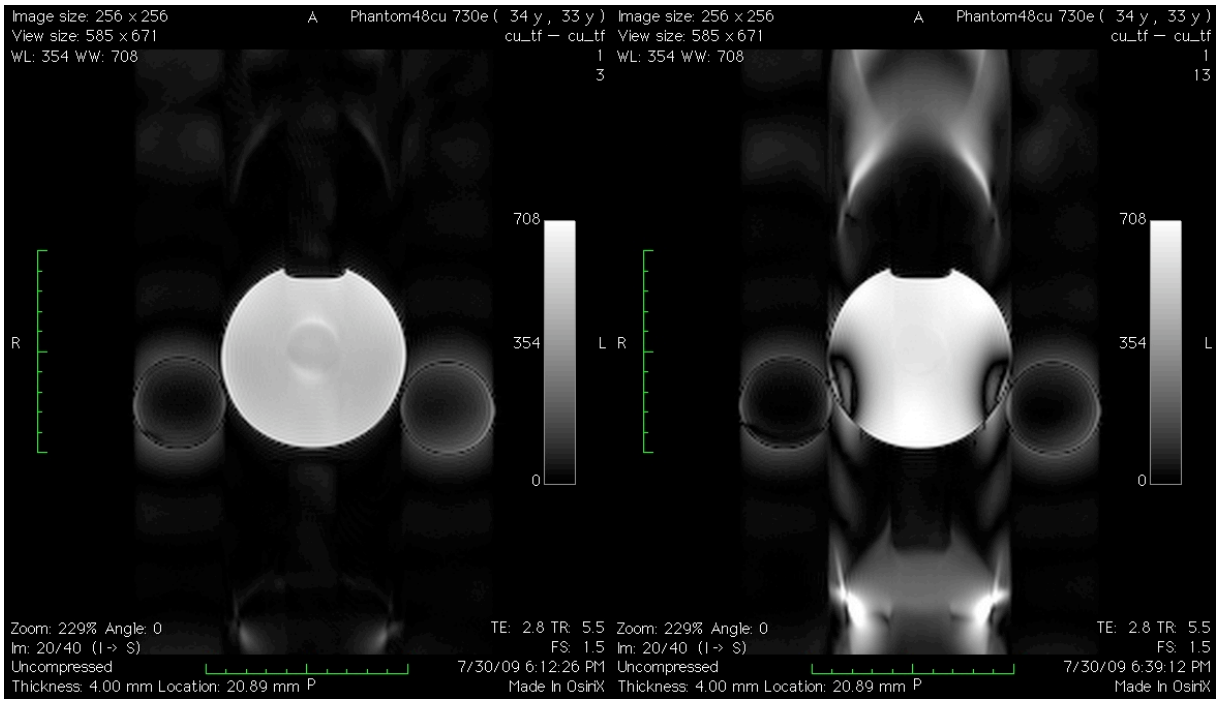

Figure 5.18 To the left a fat-saturation TR-length with the factor 1.6 and to the right a factor of 3.0 times the image-acquisition TR

Even if it in theory would be desirable to increase the fat-saturation TR-length to narrow the bandwidth of the pulse, in practice additional artefacts occur. Figure 5.18 shows the images for a fat-saturation TR factor of 1.6 to the left and 3.0 to the right. It reveals that the fat-suppression increases while the water signal intensity is less affected, but the artefacts from and in the water object increase.

5.10 Optimization of the fat-saturation flip angle pulse

For an optimal fat-saturation a flip angle of 180° is often not needed. Additionally a reduction of the fat-saturation flip angle is expected if several fat-saturation pulses are gapplied in a significant shorter interval than 200 ms. This is the case with pairing where the fat-saturation pulse is repeated after one TR of approximately 5 ms.

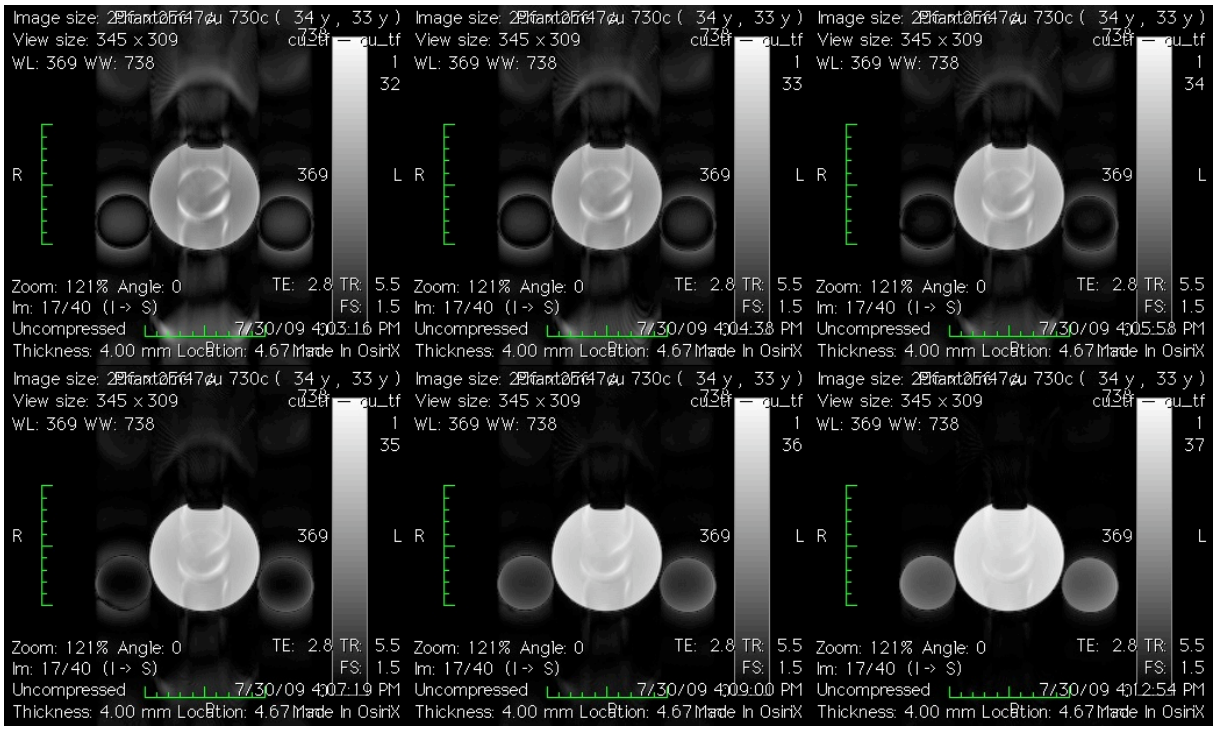

Figure 5.19 Series with reduction of the fat-saturation flip angle in activated pairing from 90° top left to 40° bottom right by steps of 10°

The series of measurements with varying flip angles of the fat-saturation pulse in pairing-setup is shown in Figure 5.19. Where the pulses in the two TR's are similar, the series has a variation from 90° to 40° in steps of 10°. It shows the best result with a flip angle of 70°. It is noticed that there is still a slight fat-saturation left even at a flip angle of 50°.

5.11 Flip angle variation with only one fat-saturation pulse in the pairing block

To demonstrate the effect of double fat-saturation pulse in the pairing block on the fat-saturation another series of images with flip angle variation was taken, where only one fat-saturation pulse was played out during the pairing block of two TR's.

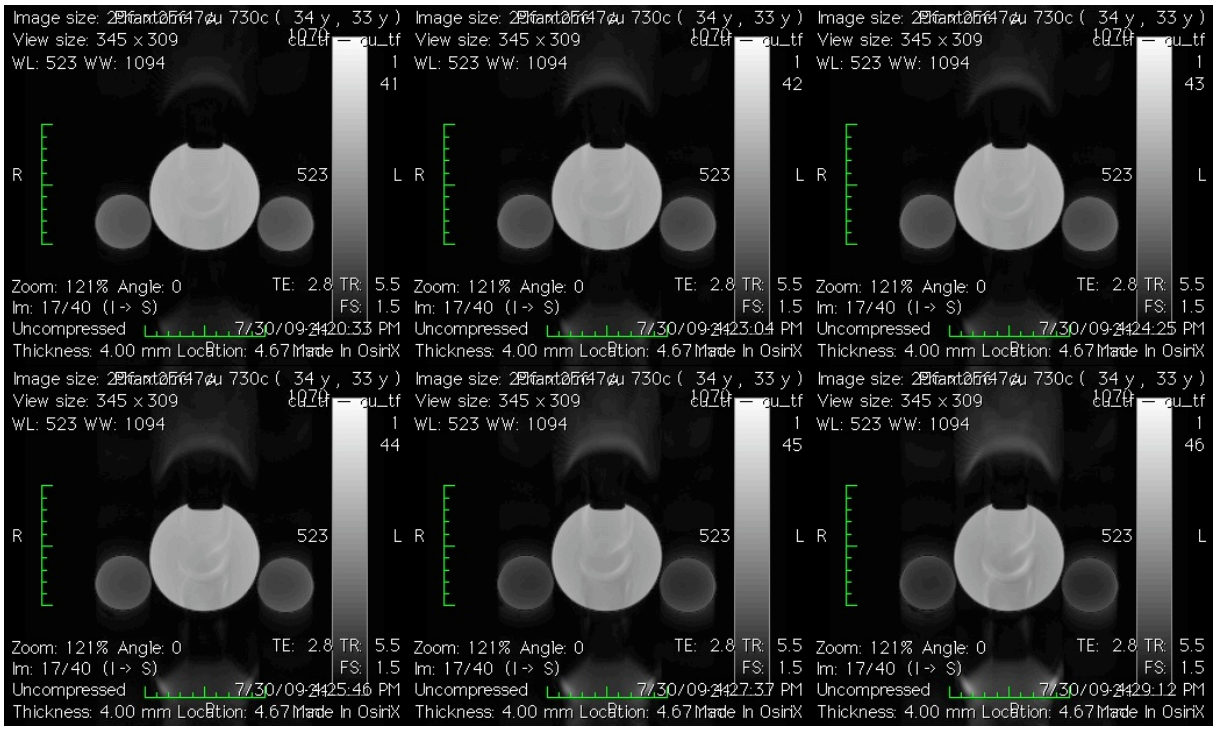

Figure 5.20 Flip angle variation with either an fat-saturation pulse in the first or the last TR in the pairing fat-saturation block, according to the scheme Flip1,Flip2: top left 60°,0°; 70°,0°; 80°,0°; 0°,70°; 90°,0°; 0°,90° bottom right

The series of the single fat-saturation pulse in the pairing block in Figure 5.20 at the range of 60° to 90° reveals that a slight fat-saturation effect is first recognized at a flip angle of 90°. The order of the pulse whether the pulse is played out in the first TR or the second has no influence of the result.

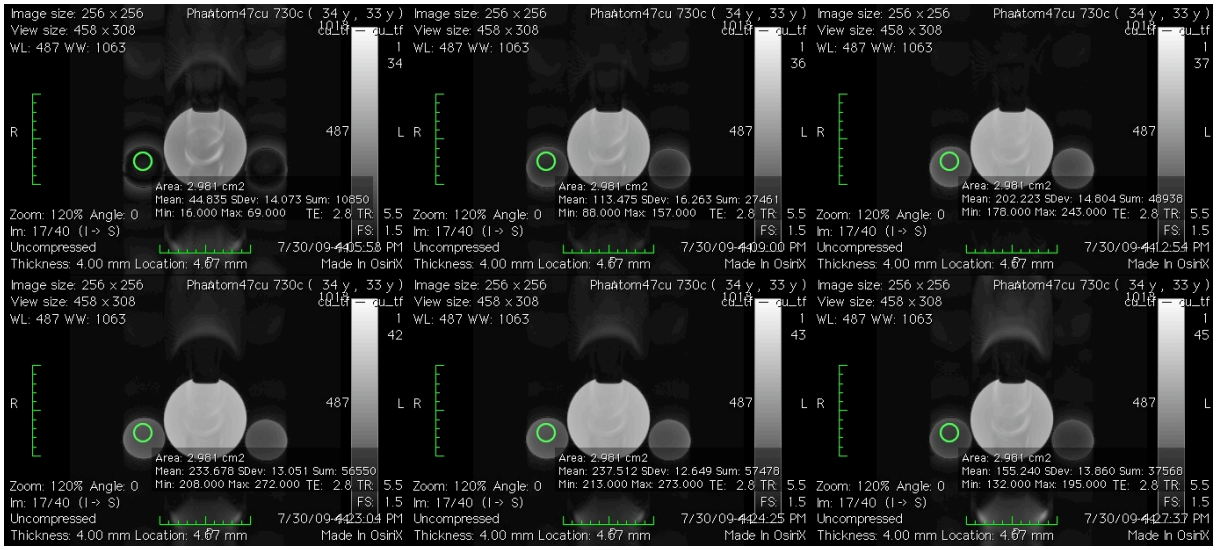

Figure 5.21 Series with double fat-saturation pulses at the top from left to right at 70°, 50° and 40°; at the bottom single fat-saturation pulse in the pairing block from left to right 70°, 80° and 90°. The region of interest in the images is copied and placed at the exact same position.

In Figure 5.21 a comparison of single and double fat-saturation pulse in the pairing block is performed. The intensity of the fat is measured by regions of interest (ROI) at exact same position. The measurement reveals that two 40° pulses are more effective than one 80° pulse. The fat-intensity of the double 40° pulse saturation is 17% lower than the single 80° pulse saturation.

5.12 Influence of the pairing on the fat-saturation

To show the influence of pairing on the fat-saturation a measurement series with only one fat-saturation TR has been performed.

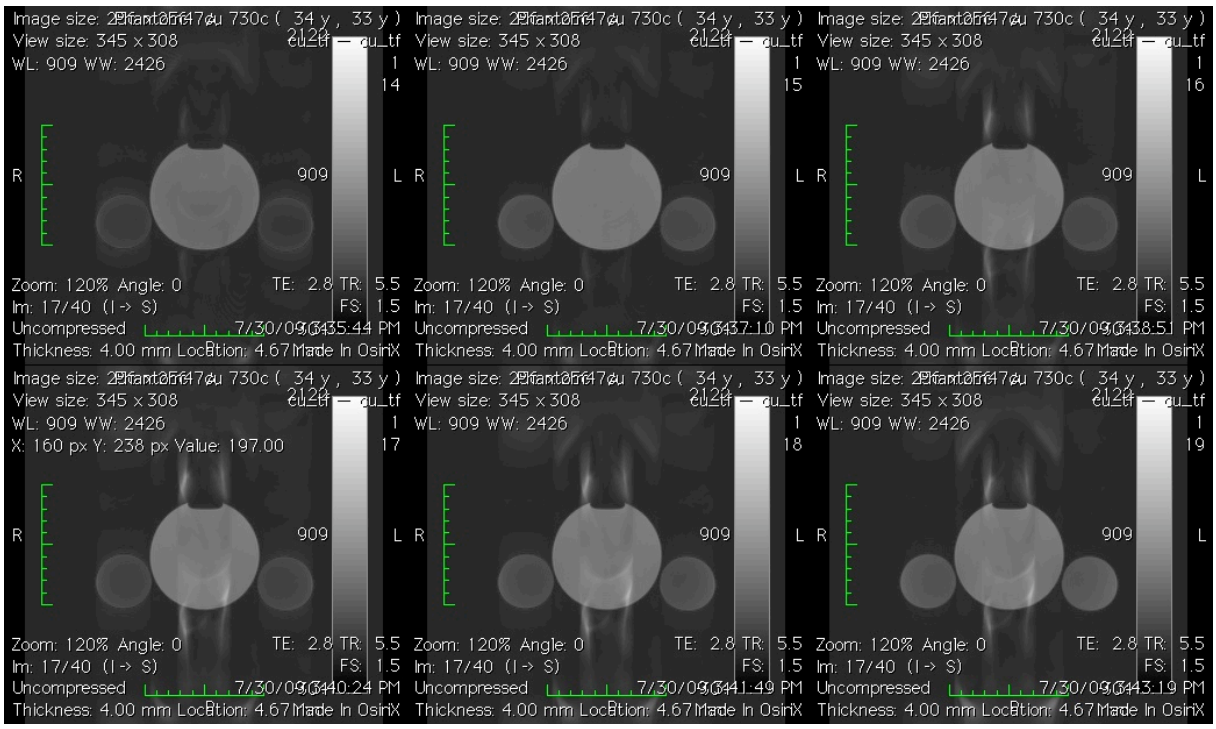

Figure 5.22 Series without pairing and only one TR increasing the fat-saturation TR from the factor 1.0 of the imaging TR at top left increased by 0.2 to 2.0 at bottom right. The moment of the spoiler gradients kept constant 0,4π, while the fat-saturation pulse increases.

Figure 5.22 shows the same series with lengthening of the fat-saturation TR as in Figure 5.17 with the difference of only one fat-saturation TR in each block and no pairing. It is obvious, that the fat-saturation is not as efficient as in Figure 5.17, which can be explained by only one fat-saturation pulse at the same flip angle during both series and with the knowledge of the results in the chapter above. Nevertheless, the background noise is higher and the water-signal is lower, which results in a lower signal to noise ratio.

5.13 Variation of the spoiler-gradient scheme in one pairing block

A series with variation of the spoiler gradient scheme was initially planed to estimate whether a steady state of the fat-signal occurs due to the two fat-saturation pulses in a pairing block. The variation is done by changing the polarity of one or more spoiler de-phaser gradient pairs on the three spatial axes between the two TR's in a pairing block.

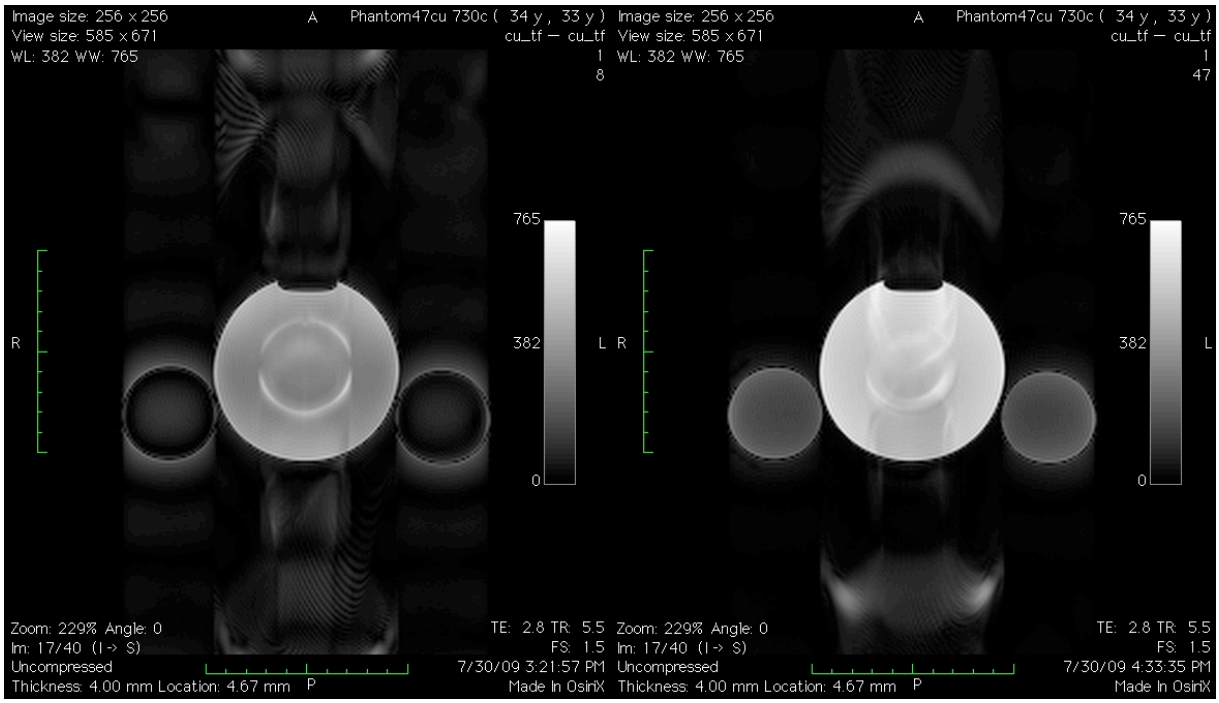

Figure 5.23 To the left standard parameters with the same spoiler gradient scheme in the pairing block. To the right same parameters as in the image to the left unless the changed polarity of one spoiler gradient pair

Figure 5.23 reveals that a change in the spoiler gradient variation gives a less effective fat-saturation and even slightly more eddy current artefacts.

5.14 Comparison of the self-programmed and the product sequence on a human knee

The previous measurements have been performed on a phantom, which is preferable to compare the artefacts reliably. To get an impression of the affection from the artefacts on medical images a series of images on a knee from a healthy volunteer have been acquired.

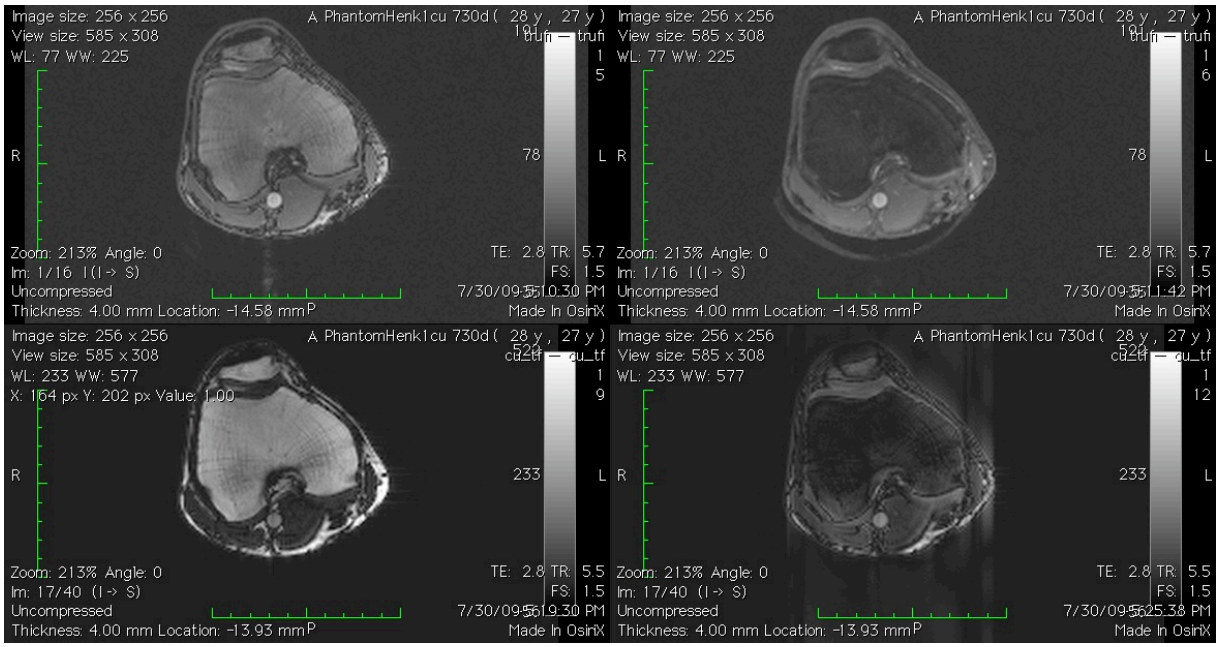

Figure 5.24 Top row product TrueFisp images, to the left without fat-saturation and to the right with fat-saturation. Bottom row self-programmed TrueFisp images, to the left without fat-saturation and to the right with fat-saturation

Figure 5.24 shows those images. At top-row are the images from the product TrueFisp sequence with a fat-saturated image to the right. At the bottom-row the images of the self programmed sequence with the pairing-based fat-saturation at the right.

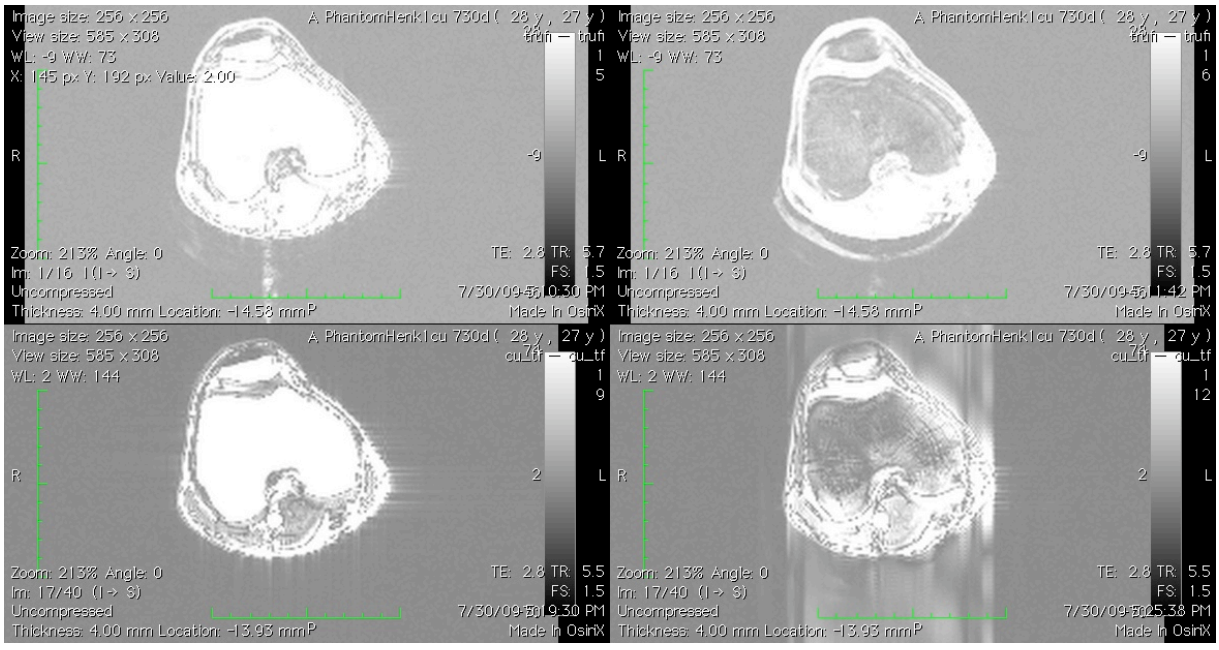

Figure 5.25 Same acquisition as in Figure 5.24 but, window levelled to contrast enhances the air space and noise. Top row product TrueFisp images, to the left without fat-saturation and to the right with fat-saturation. Bottom row self-programmed TrueFisp images, to the left without fat-saturation and to the right with fat-saturation

The same images as in Figure 5.24 are shown in Figure 5.25. Further, in the last images, the window level is adjusted to enhance the airspace and artefacts. Comparing the two unsaturated images there are similar artefacts with only slightly more enhanced speckles at the border between the knee and the surrounding airspace. The fat-saturated image from the self-programmed sequence shows a sufficient fat-saturation,

most obvious in the bone marrow of the femur and patellae. Nevertheless there are some additional artefacts with smeared signal in a vertical band over the image. This looks like the artefacts from the oil bottles in the phantom images and hence corresponds most likely to fat-signal reintroduced to the k-space due to insufficient spoiling. The image would be able to reveal pathologic findings like bone-marrow oedema but doesn't reach the quality needed for clinical imaging.

6 Discussion

As shown in Figure 5.24 and Figure 5.25 the self programmed balanced SSFP sequence has more artefacts both in the fat-saturated image and the none-saturated image than the product TrueFisp. The difference in the non-saturated image is only slight. The fat-saturation with pairing is successful but doesn't deliver images that can be used for diagnostic purpose. The difference in the artefacts in the images of the self-programmed sequence and the product sequence can have different reasons. One of the technical reasons could be the structure of the IDEA FLASH sequence, which is the base for the self programmed balanced SSFP sequence. The design of the pulses and the gradients is not so sophisticated and more static in the IDEA FLASH than in the product sequence. The IDEA FLASH is only one file focused on consistency, while the product sequence is a collection of files and methods with sophisticated optimization routines for the objects such as gradients and pulses. Even the method to reach the equilibrium differs with pre-scanning and the constantly fading amplitude of the α-pulse during the pre-scanning instead of an initial $\alpha/2$-pulse as used in the self programmed sequence. These technical differences might also be an explanation as to why there already are some artefacts in the IDEA-FLASH fat-suppression as shown in Figure 5.2 and Figure 5.3, even if it should be easier to produce less artefacts in a spoiled sequence such as the FLASH than in a balanced sequence such as the product TrueFisp-sequence.

Another technical source for artefacts is the scheme of the passing track through the k-space. As shown in Figure 5.8 a constant line readout direction produces clearly more artefacts – which without fat-saturation are not visible in images windowed as for medical use – than with meandering line direction. These artefacts might be produced by the jumps of the gradients, which are minimized in the meandering readout scheme. These artefacts correspond to eddy current artefacts.

Figure 5.12 and Figure 5.13 give some information about the artefacts produced by the fat-saturation pairing block. The image in the upper left corner gives the impression of two different artefacts in the image. One is a general blurring of the image related to the fat-signal most intensive over and under the oil bottles. Another one, over and under the water phantom, is similar to the eddy current artefact in the image to the left in Figure 5.13. After deactivation of the fat-saturation pulse but otherwise constant gradients, pulses and TR in the pairing block, the blurring artefact from the fat-signal vanishes, shown in the image upper right corner Figure 5.13. In this image only the eddy current artefact occurs. Increasing the moment of the spoiler gradients – still with deactivated fat saturation pulse – increases the eddy current artefacts, shown in the lower left image in Figure 5.13. If both the spoiler gradients and fat-saturation pulse are deactivated - but else constant gradients, pulses and TR in the pairing block – the eddy current artefact vanishes and the result is similar to the image without pairing to the left Figure 5.8. It is noticed that the pairing block at the acquisition of the images in Figure 5.12 and Figure 5.13 had a TR extended by the factor 1.6 to the image acquisition TR. This shows

that the pairing prohibits a disturbance of the steady state even if the image-TR and pairing-TR are unequal. But the eddy current artefacts are still disturbing the image acquisition even if the gradient action causing the eddy currents is located inside the pairing block. But Figure 5.23 shows a certain reduction of the eddy current artefacts from the pairing. The comparison of Figure 5.22 – series without pairing – and Figure 5.17 – a series with pairing – shows even a benefit of the signal to noise ratio of the pairing.

The other artefact component, the blurring of the fat-signal, in the image upper left corner Figure 5.13 can be caused by fat-signal that is either insufficiently spoiled or reintroduced to the k-space by the unselective α-pulse. During the acquisition of the images in Figure 5.13 a spoiler moment of $0.4*2\pi$ was used. The reason for the low spoiler moment was the limitation of the TR. Even if the pairing in theory permits an extension of the pairing TR, in practice artefacts limit the amount of extension. Figure 5.18 shows in the image to the right an extension of the pairing-TR to 3 times the imaging-TR. Even if this gives a more sufficient reduction of the fat-signal and a higher signal of the water-phantom due to the longer and hence more selective saturation pulse, the resulting image is more affected by artefacts. This is why the spoiler gradient moment is reduced to $0.4*2\pi$, otherwise the pairing-TR would increase significantly or the fat-saturation pulse duration would decrease resulting in a more unselective saturation pulse. The value of $0.4*2\pi$ is already a compromise between selectivity and artefacts due to insufficient spoiling at a constant pairing TR of 1.6x imaging TR. This is shown in the Figure 5.14.

With the initial intention to investigate a possible own steady state of the fat signal, a series with variation of the spoiler gradient scheme was performed. I.e. the polarity of the spoiler pairs in-between the two TR's of a pairing block were changed. The image to the right in Figure 5.23 shows the result, with a reduction of the fat-suppression by variation – i.e. dissimilar TR-actions in one pairing block – of the spoiler gradient polarity. An approach to increase the spoiling of the fat-signal was a RF-spoiling with a fat-suppression pulse at different phases, but Figure 5.15 and Figure 5.16 shows that RF-spoiling of the fat-suppression pulse has no influence on the result.

As mentioned in the theory chapter a flip angle of 180° is not necessary for an optimal fat-saturation and most of the times the angle is by far lower than 180°. The series with variation of the flip angle, with otherwise constant parameters shows, as seen in Figure 5.19, the best result for a flip angle of 70°. Figure 5.21 reveals that it is more effective to apply two pulses of 40° during a pairing block rather than applying one fat-saturation pulse of 80° during the pairing block with two TR's. The pairing with two similar TR's does not only reduce the artefact but also gives a synergetic effect of the fat-saturation where two similar pulses give a higher reduction of the fat-signal than one single pulse with the double flip angle and hence a higher SAR as the two smaller ones. There is so far no reasonable explanation for this synergetic effect.

The series for the optimization of the TR-length, with otherwise constant parameters, shows in Figure 5.17 an optimum of the pairing TR-duration at a multiplication factor of 1.6 of the imaging TR. The series is only documented by images from the range of 1.0 to 2.0. At higher factors the, most likely, eddy current artefacts compromises the image quality as shown in Figure 5.18. It is noticed that the fat-saturation has to local minima of the fat signal reduction at the factor 1.0 and 1.6, and even another one not shown in

this figure will appear at the factor 2.3. Even this phenomenon has no reasonable explanation.

Initially a more conventional fat-saturation scheme was planned with a pairing fat-saturation block after a fixed number of imaging TR's. Figure 5.10 shows the result and reveals that with increasing number of intermitted fat-saturation blocks the artefacts increase. Even this time the artefacts look like the eddy current artefact in Figure 5.8, which gives the suspicion that the eddy current artefact is summarized from the pairing blocks. Due to that fact a series with only one fat-saturation pairing block at each readout line was performed. Figure 5.11 shows the result and the best localization seems to be just before the imaging TR in the centreline of the k-space, which gives the best compromise of artefacts to fat-signal reduction. As expected from this scheme the contour of the fat-object is still visible as a slim signal intense line. Eventually this contour could be saturated by a few saturation pulses in the periphery of the k-space line. Compared to a more conventional scheme with a saturation block after a fix number (after every 8^{th} TR) this scheme would have a potential to save SAR.

The empiric investigation of the parameters have given the best result for a pairing TR of 1.6 times the imaging TR, which in the self programmed balanced SSFP sequence outgoing from the IDEA-FLASH was the achieved minim TR of 5.5 ms, hence a pairing TR of 8.8 ms. The moment of the spoiler gradient gave the best compromise at a moment of $0.4*2\pi$. For this pairing TR and spoiler gradient moment the best compromise between water signal affection and fat-signal reduction was achieved with an off-set frequency of the saturation pulse of 12ppm. The best result for the flip-angle was 70° in both pairing TR.

With those parameters an image of a knee was performed which is shown in Figure 5.24. It is noticed that the offset frequency in this image was changed and adapted to fat, which has a slightly different offset frequency than oil, which was used in the phantom for the empiric investigation. The fat-saturated image achieved with the self-programmed balanced SSFP sequence suffers mainly under a smeared signal, which looks like the artefact from the oil bottle in the image to the upper left in Figure 5.12 and Figure 5.13. This might hence be artefacts from insufficiently spoiled fat-signal. A reduction of this smeared fat-signal could possible be achieved by multiple numbers of acquisitions. The option of increasing NA is implemented in the IDEA-FLASH but was difficult to keep working properly after programming the reordering of the acquisition scheme to a meander path. The effort to re-establish the option hasn't been made because it seems not useful for a balanced SSFP sequence. Most of the specific applications for the balanced SSFP sequence are fast examinations of moving objects like cardiac imaging where multiple NA would give artefacts when the repeated movement is taking a slightly different path in every cycle.

The empiric investigation implies some drawbacks for this multi parametric optimization. Hence, only one parameter can be changed at a time to verify the parameter effect on the resulting image. Handling of related parameters, which might get another optimum due to a change of correlated parameters, is difficult. A simulation in an iterative model might give better results. It even could reveal the origin of the two unexplained effects of synergy of doubled fat-saturation pulses and the multiple local minima of fat-signal under variation of the fat-saturation-TR.

7 Conclusion

The first step of the programming, to change the IDEA-FLASH, which is a spoiled gradient echo sequence, into a balanced SSFP sequence was successful and gave similar results as the product TrueFisp sequence. Even the implementation of a pairing based frequency selective fat-saturation succeeded. The best result for the fat-saturation was with the minimum imaging TR of 5.5ms at a pairing TR of 8.8ms; a spoiler moment of $0.4*2\pi$; a flip-angle of 70° and a position of the pairing-block just in front of the centre k-space line after 127 imaging TR´s in a 256 matrix. Nevertheless the result of the fat-saturated image was not useful due to massive artefacts, which has mainly three factors. The smallest influence might be the – compared to the product sequence – none optimized IDEA-FLASH base-sequence. To implement the pairing in the product sequence would have been beyond the scope of a master thesis. Eddy currents might cause the major parts of the artefacts. The pairing might reduce the eddy current artefacts but, for the fat-saturation, not sufficiently. This causes a reduction of the pairing TR length, with a compromise of reducing the spoiler gradient moment to avoid a too short and hence too unselective fat-saturation pulse. The reduced spoiling might be the reason for fat-signal components spread out on the image. This implementation revealed two unexplained phenomena. The first one is a synergetic effect of two fat-saturation impulses given in shorter period compared to one pulse with a double flip angle, where the doubled smaller pulses results in a higher signal reduction of the fat. The other phenomenon is a periodic variation of the fat-signal reduction by continuously increasing the pairing TR. To reveal an explanation of those phenomena a numerical simulation could be of great value.

8 References

1.) Bieri O, Markl M, Scheffler K. Analysis and Compensation of Eddy Currents in Balanced SSFP. Magn Reson Med 2005;54:129-137

2.) Hanson LG. Is Quantum Mechanics Necessary for Understanding Magnetic Resonance? Concepts in Magnetic Resonance Part A 2008;Vol. 32A:329-340.

3.) Levitt MH. Spin Dynamics: Basics of Nuclear Magnetic Resonance. 2nd ed. 2008 Wiley, ISBN 978-0-470-51117-6

4.) Nishimura DG. Principles of Magnetic Resonance Imaging. Course compendium EE 369B Spring Quarter 1994-95

5.) Bernstein MA et al. Handbook of MRI Pulse Sequences. 2004 Elsevier Academic Press, ISBN978-0-12-092861-3

6.) Vlaardingerbroek MT, Boer den JA. Magnetic Resonance Imaging: Theory and Practice. 3rd ed. 2003 Springer, ISBN 3-540-43681-2

7.) Rummeny et al. Ganzkörper-MR-Tomogrphie. 2002 Thieme, ISBN 3-13-125011-9

8.) Stöcker. Taschenbuch der Physik. 2007 Wissenschaftlicher Verlag Harri Deutsch, ISBN978-3-8171-1720

9.) Bracewell RN. The Fourier Transform and its Aplications. 3rd ed. 2000 Mc Graw Hill, ISBN 0-07-116043-4

10.) Chavhan GB et al. Steady-State MR Imaging Sequences: Physics, Classification, and Clinical Applications. RadioGraphics; 28:1147-1160

11.) Cheng DK. Fundamentals of Engineering Electromagnetics. 1993 Addison Wesley, ISBN 0-201-60071-4

12.) Bieri O. Personal communication. MR Physics at the Department of Medical Radiology, University Basel, Basel 2008-2009

13.) Scheffler K. Personal communication. MR Physics at the Department of Medical Radiology, University Basel, Basel 2008-2010

14.) Siemens Training and Development Center Cary, North Carolina, USA . IDEA Sequence Programming Course Syllabus

15.) Zaitsev M. Parameter Map; Oral presentation, at IDEA User Meeting, Tübingen 2004